APPENDIX

APPENDIX A

The BESS Operating Result

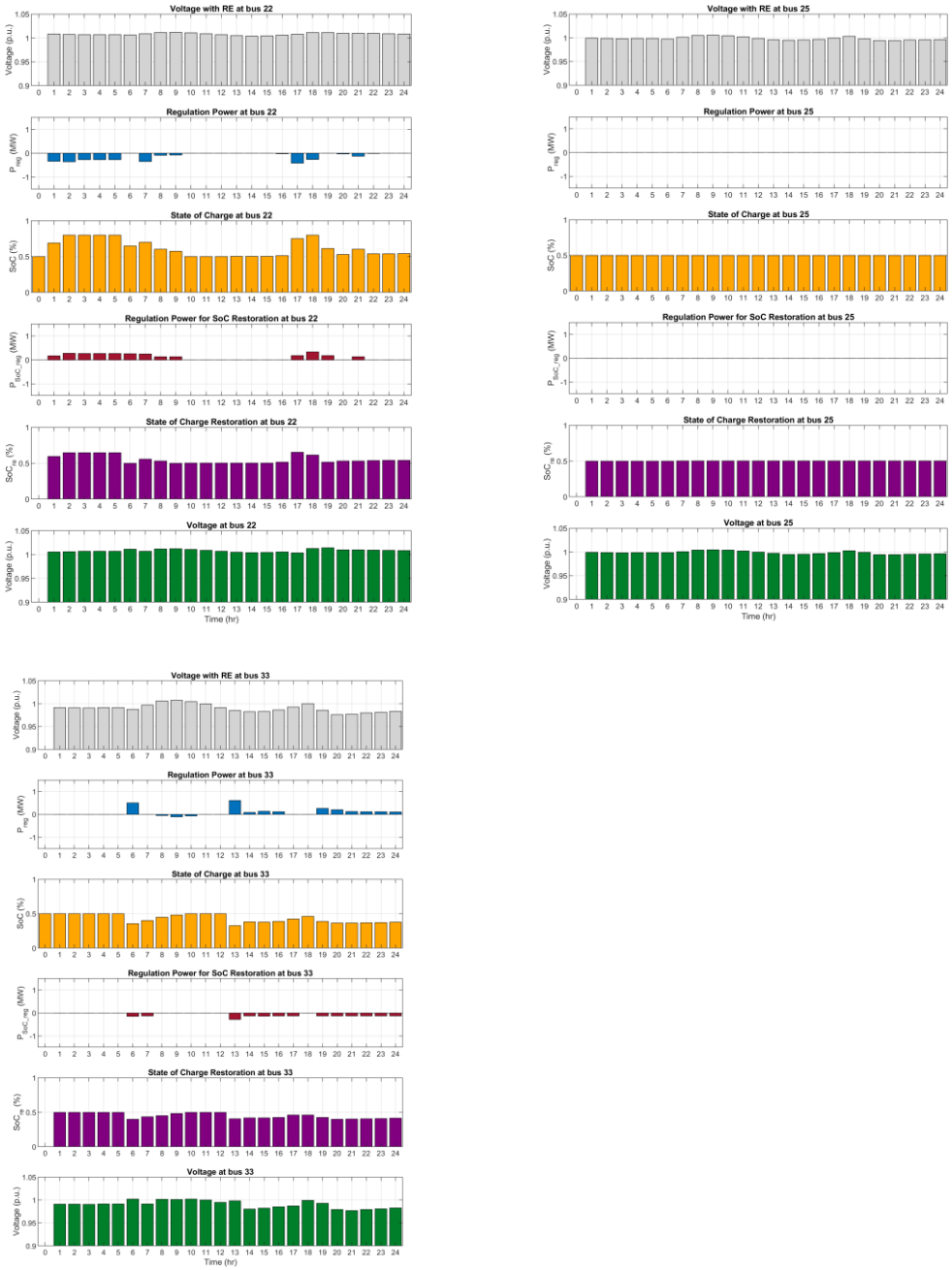

Figure A.1 Time-Series Profiles of Voltage, Regulation Power and Battery SoC at Bus 22, 25 and 33 in IEEE 33-bus system Scenario 1

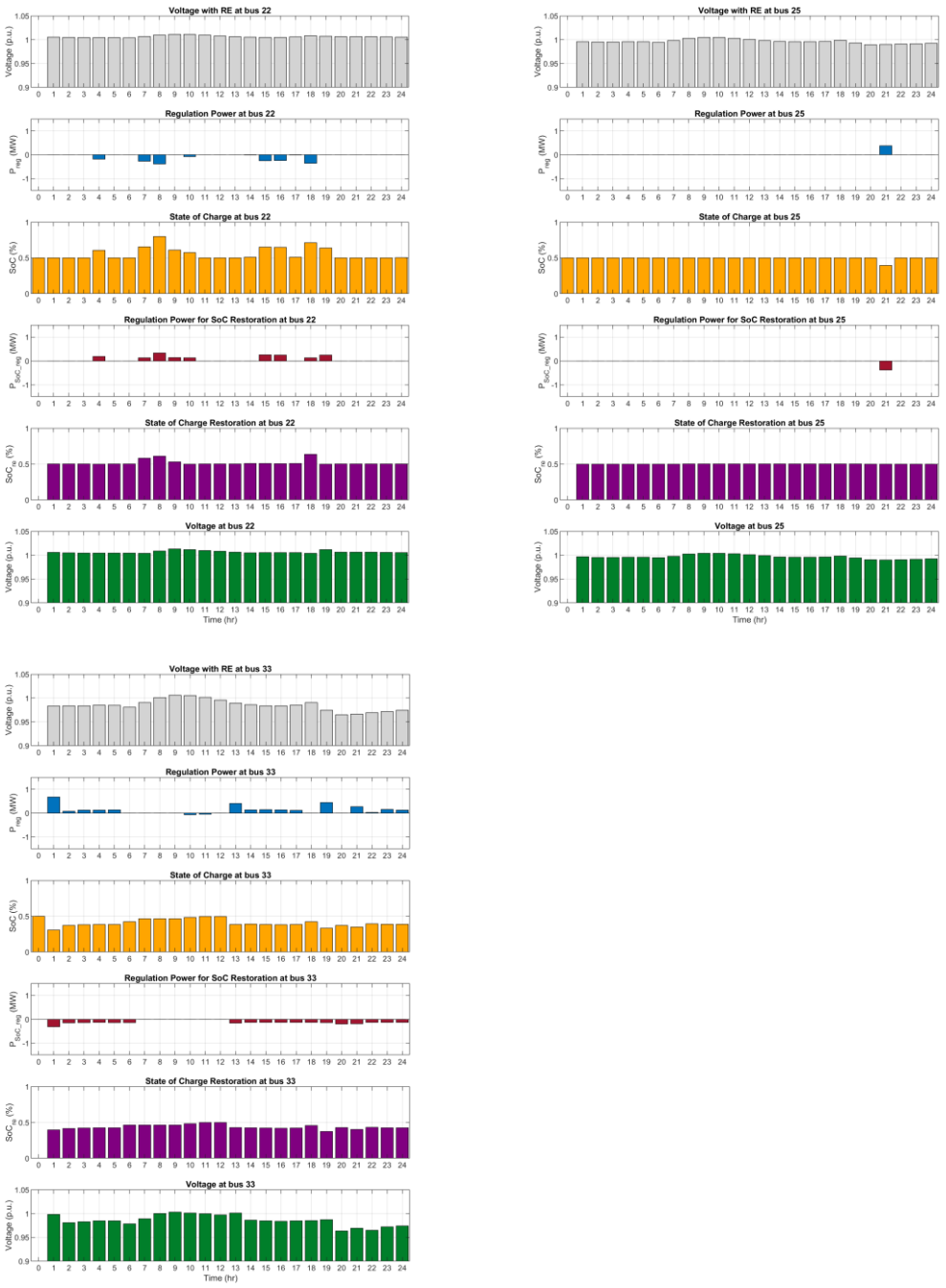

Figure A.2 Time-Series Profiles of Voltage, Regulation Power and Battery SoC at Bus 22, 25 and 33 in IEEE 33-bus system Scenario 2

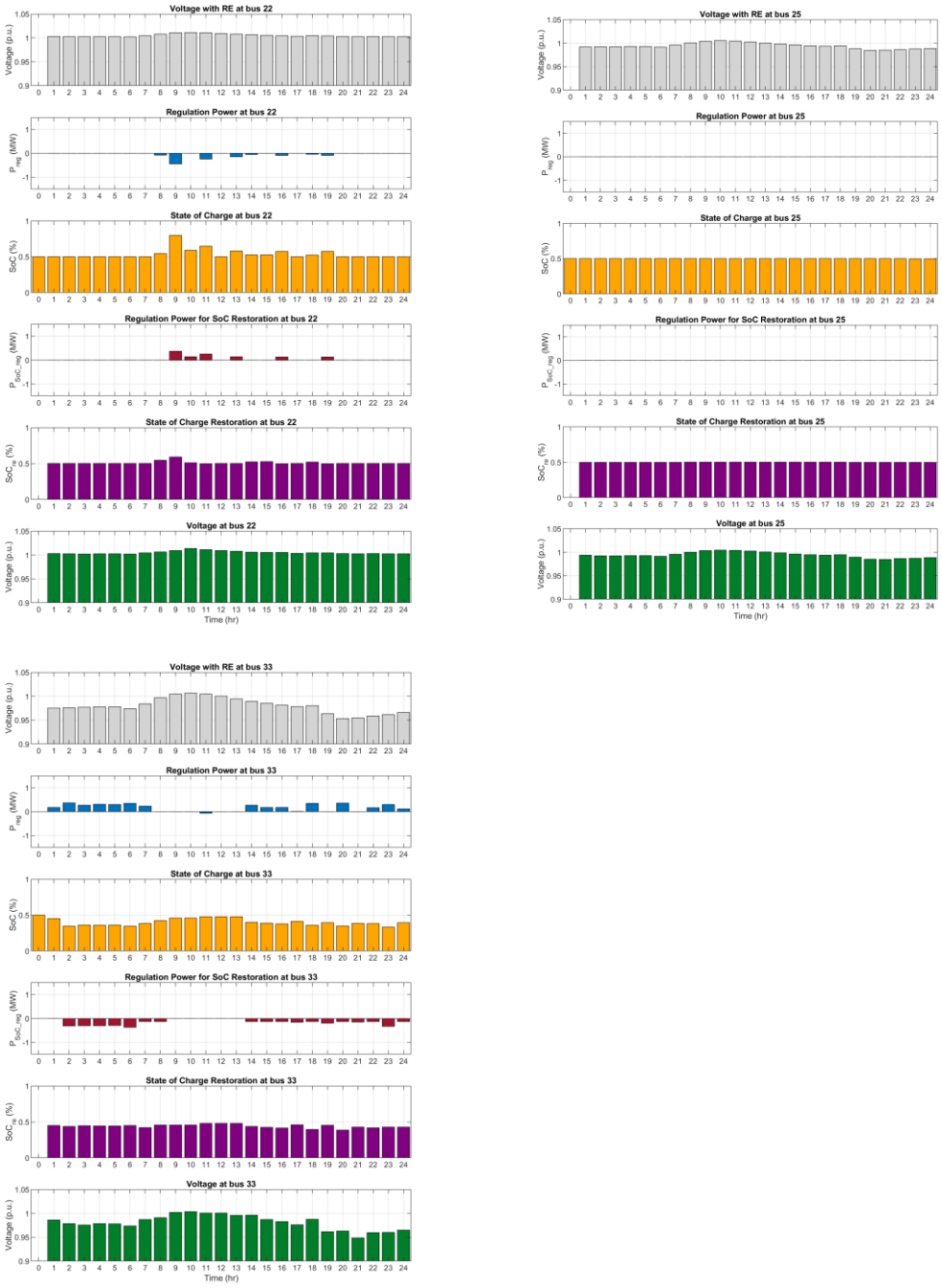

Figure A.3 Time-Series Profiles of Voltage, Regulation Power and Battery SoC at Bus 22, 25 and 33 in IEEE 33-bus system Scenario 3

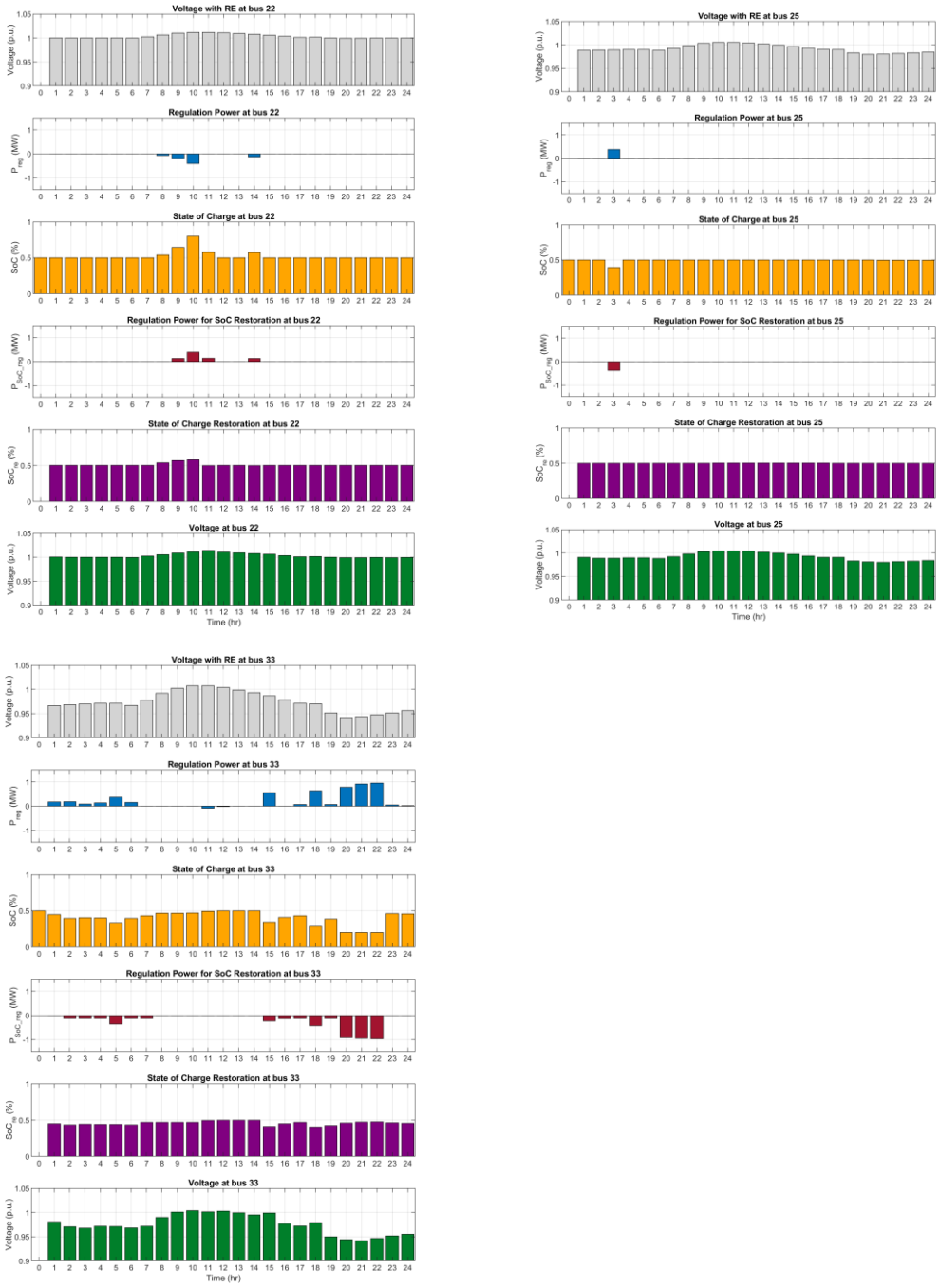

Figure A.4 Time-Series Profiles of Voltage, Regulation Power and Battery SoC at Bus 22, 25 and 33 in IEEE 33-bus system Scenario 4

Figure A.5 Time-Series Profiles of Voltage, Regulation Power and Battery SoC at Bus 22, 25 and 33 in IEEE 33-bus system Scenario 5

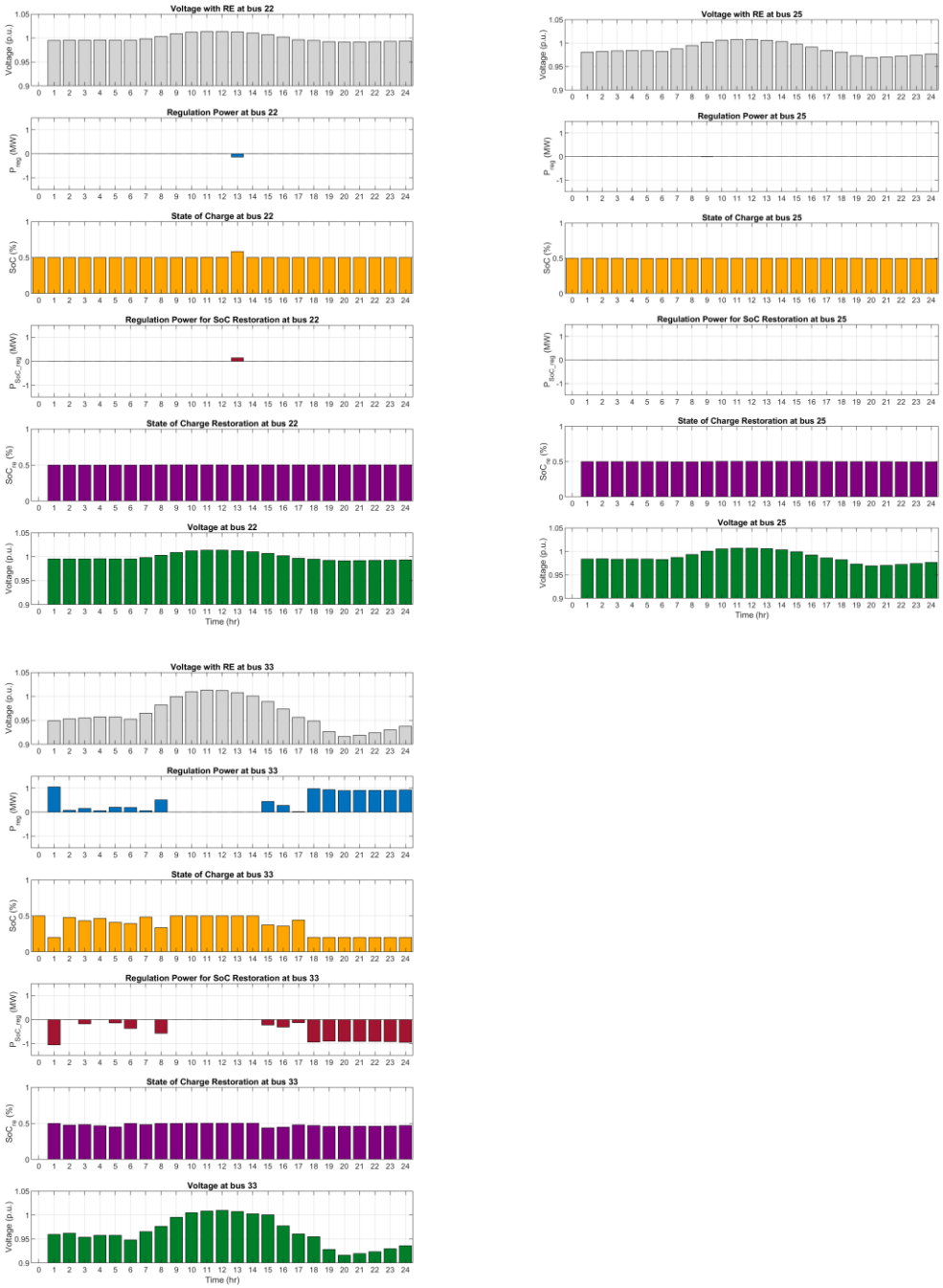

Figure A.6 Time-Series Profiles of Voltage, Regulation Power and Battery SoC at Bus 22, 25 and 33 in IEEE 33-bus system Scenario 6

Figure A.7 Time-Series Profiles of Voltage, Regulation Power and Battery SoC at Bus 27, 35, 46 and 50 in IEEE 69-bus system Scenario 1

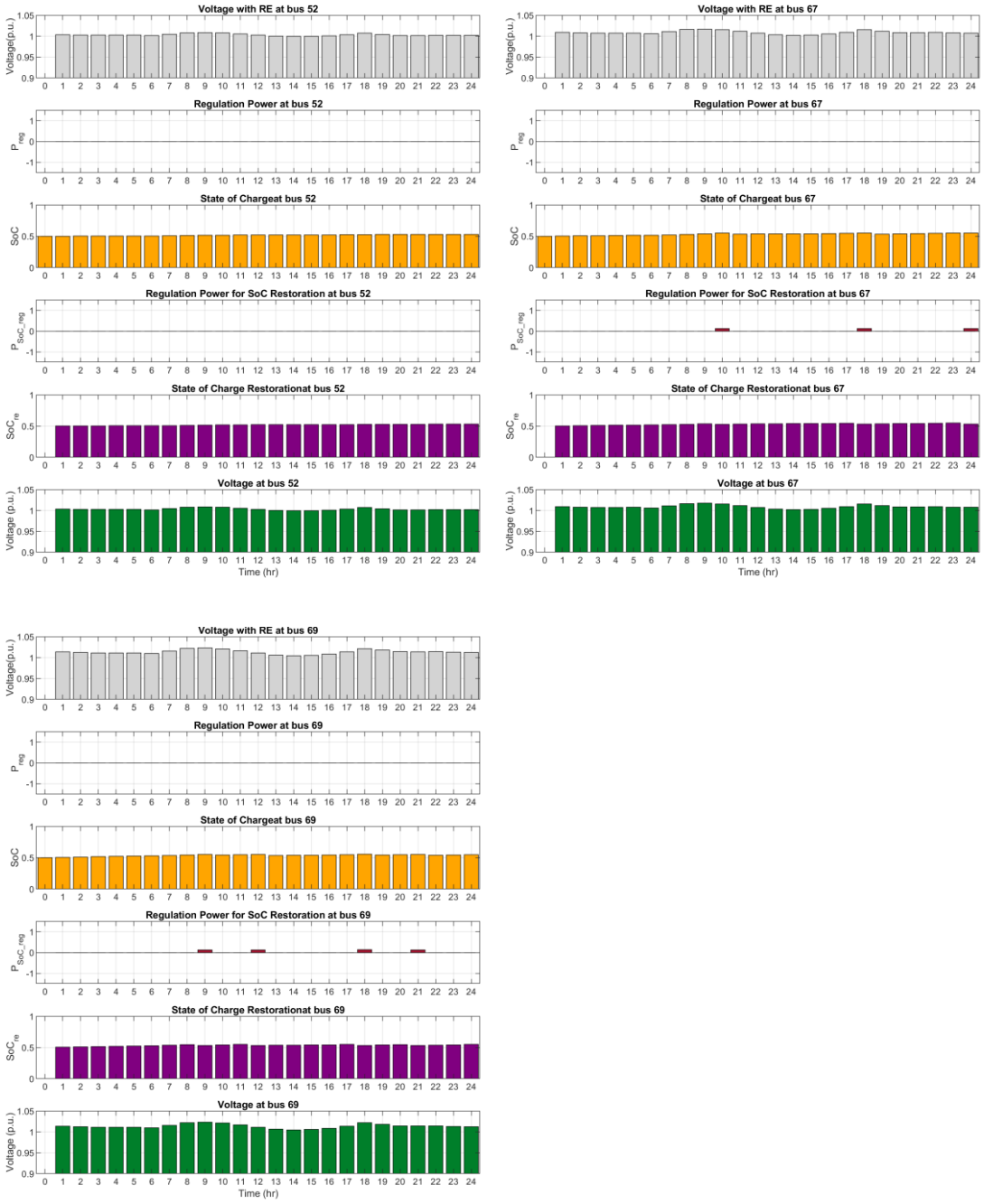

Figure A.8 Time-Series Profiles of Voltage, Regulation Power and Battery SoC at Bus 52, 67 and 69 in IEEE 69-bus system Scenario 1

Figure A.9 Time-Series Profiles of Voltage, Regulation Power and Battery SoC at Bus 27, 35, 46 and 50 in IEEE 69-bus system Scenario 2

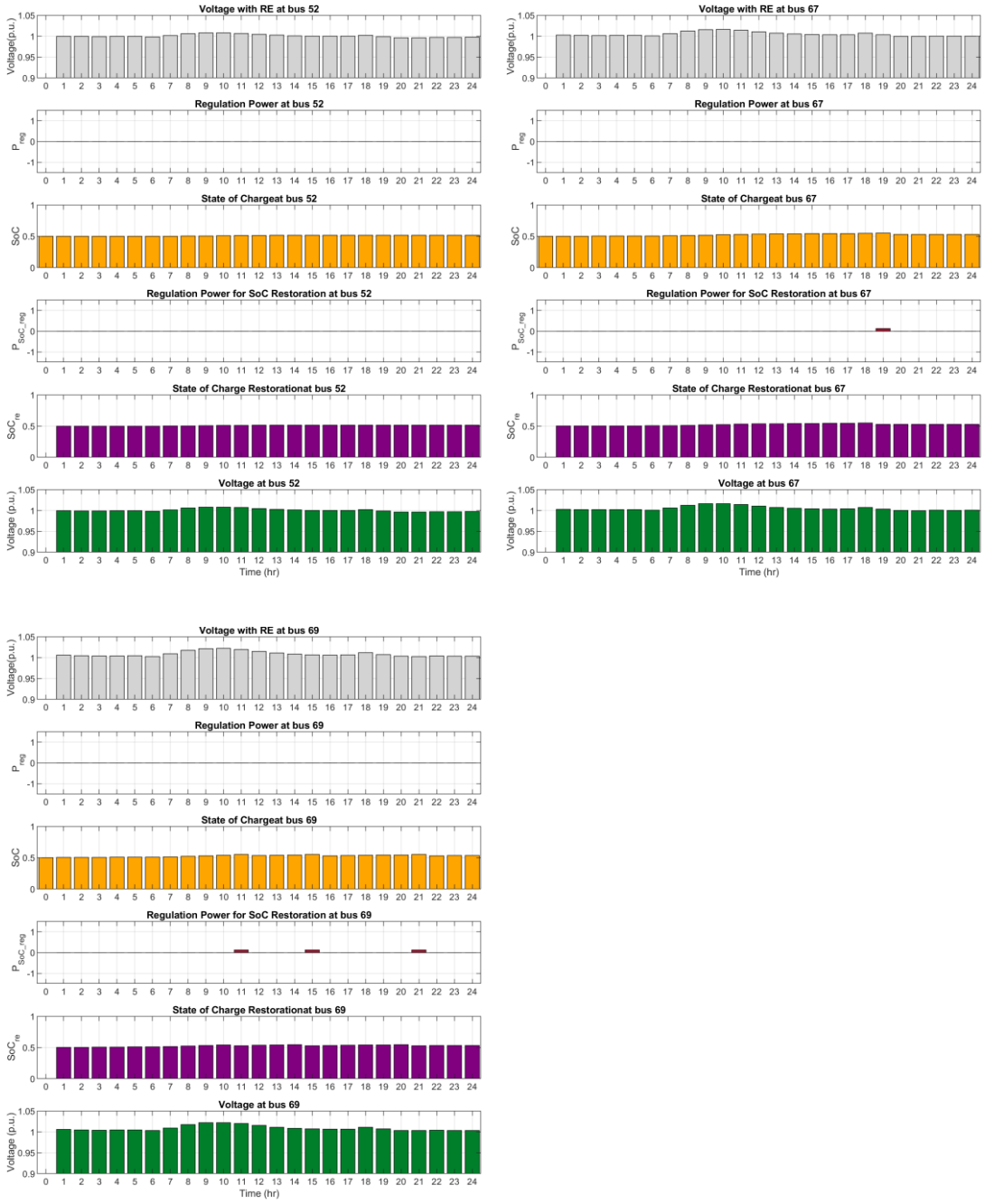

Figure A.10 Time-Series Profiles of Voltage, Regulation Power and Battery SoC at Bus 52, 67 and 69 in IEEE 69-bus system Scenario 2

Figure A.11 Time-Series Profiles of Voltage, Regulation Power and Battery SoC at Bus 27, 35, 46 and 50 in IEEE 69-bus system Scenario 3

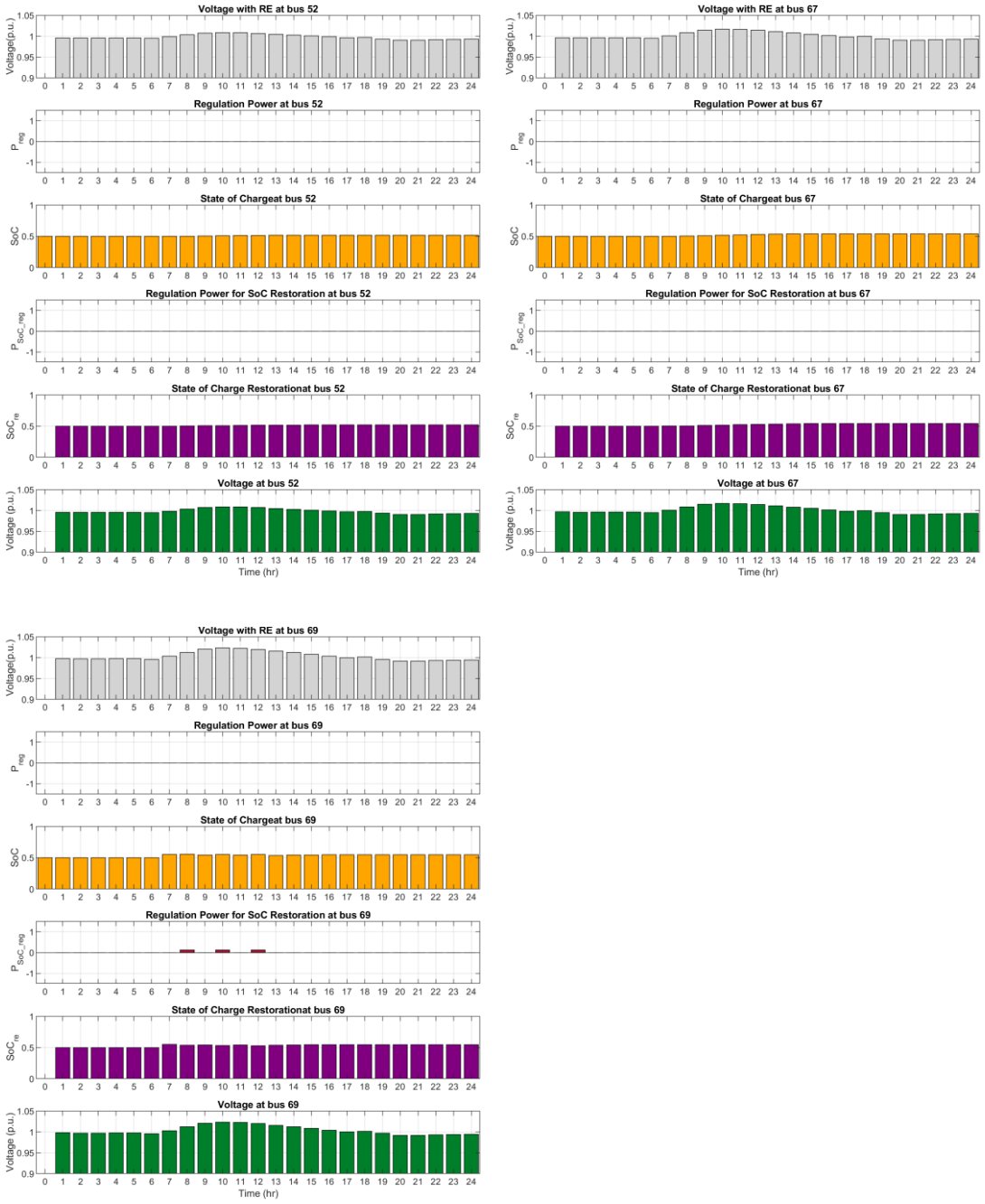

Figure A.12 Time-Series Profiles of Voltage, Regulation Power and Battery SoC at Bus 52, 67 and 69 in IEEE 69-bus system Scenario 3

Figure A.13 Time-Series Profiles of Voltage, Regulation Power and Battery SoC at Bus 27, 35, 46 and 50 in IEEE 69-bus system Scenario 4

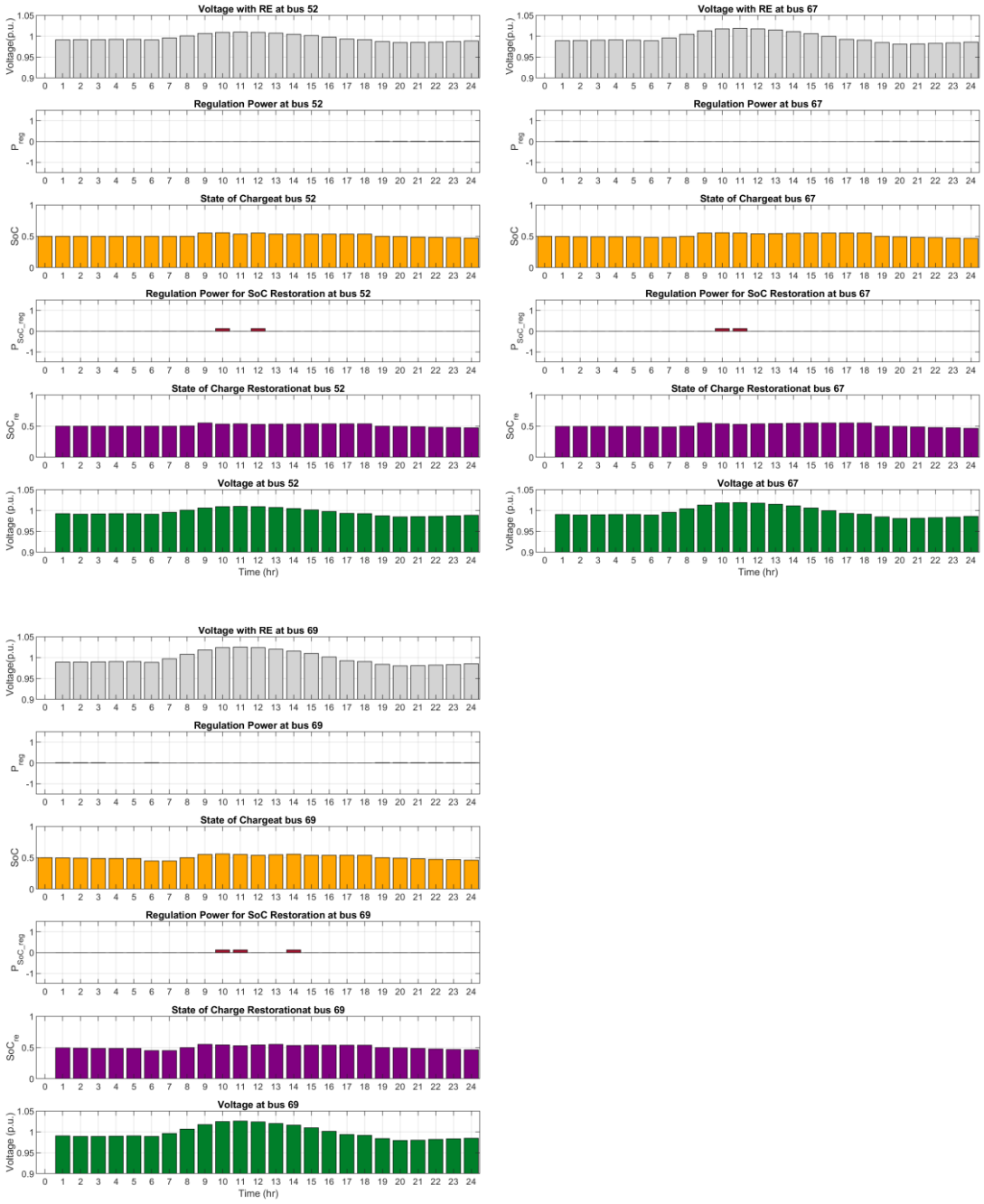

Figure A.14 Time-Series Profiles of Voltage, Regulation Power and Battery SoC at Bus 52, 67 and 69 in IEEE 69-bus system Scenario 4

Figure A.15 Time-Series Profiles of Voltage, Regulation Power and Battery SoC at Bus 27, 35, 46 and 50 in IEEE 69-bus system Scenario 5

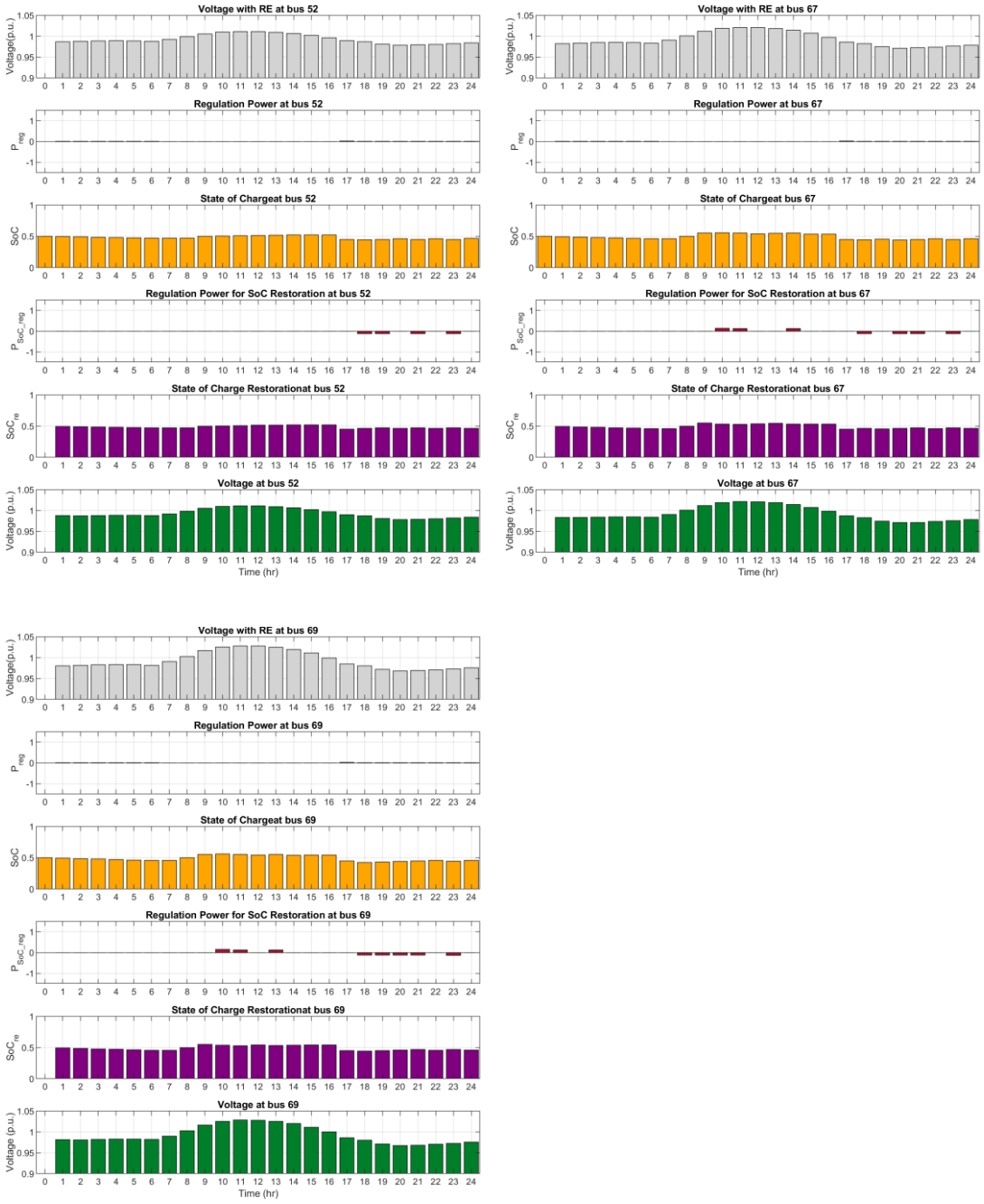

Figure A.16 Time-Series Profiles of Voltage, Regulation Power and Battery SoC at Bus 52, 67 and 69 in IEEE 69-bus system Scenario 5

APPENDIX B

Energy Profile for Test Simulation

Table B.1 Load profile

Hour	Load (p.u.)	Hour	Load (p.u.)	Hour	Load (p.u.)
1	0.6300	9	0.5132	17	0.5979
2	0.5864	10	0.5174	18	0.6374
3	0.5611	11	0.5200	19	0.8881
4	0.5348	12	0.5330	20	1.0000
5	0.5404	13	0.5506	21	0.9697
6	0.5936	14	0.5676	22	0.9192
7	0.5490	15	0.5897	23	0.8459
8	0.5139	16	0.5986	24	0.7669

Table B.2 PV profile, rated 0.25 MW

Hour	Generation (kW)	Hour	Generation (kW)	Hour	Generation (kW)
1	0.0000	9	135.7000	17	14.3000
2	0.0000	10	172.2000	18	0.0000
3	0.0000	11	185.2000	19	0.0000
4	0.0000	12	186.3000	20	0.0000
5	0.0000	13	175.6000	21	0.0000
6	0.9000	14	154.4000	22	0.0000
7	29.1000	15	119.9000	23	0.0000
8	76.0000	16	70.1000	24	0.0000

Table B.3 PV profile, rated 0.50 MW

Hour	Generation (kW)	Hour	Generation (kW)	Hour	Generation (kW)
1	0.0000	9	271.3000	17	28.5000
2	0.0000	10	344.4000	18	0.0000
3	0.0000	11	370.4000	19	0.0000
4	0.0000	12	372.6000	20	0.0000
5	0.0000	13	351.2000	21	0.0000
6	1.8000	14	308.9000	22	0.0000
7	58.3000	15	239.7000	23	0.0000
8	152.0000	16	140.3000	24	0.0000

Table B.4 PV profile, rated 0.75 MW

Hour	Generation (kW)	Hour	Generation (kW)	Hour	Generation (kW)
1	0.0000	9	407.0000	17	42.8000
2	0.0000	10	516.7000	18	0.0000
3	0.0000	11	555.6000	19	0.0000
4	0.0000	12	558.9000	20	0.0000
5	0.0000	13	526.8000	21	0.0000
6	2.6000	14	463.3000	22	0.0000
7	87.4000	15	359.6000	23	0.0000
8	227.9000	16	210.4000	24	0.0000

Table B.5 PV profile, rated 1.00 MW

Hour	Generation (kW)	Hour	Generation (kW)	Hour	Generation (kW)
1	0.0000	9	542.6000	17	57.1000
2	0.0000	10	688.9000	18	0.0000
3	0.0000	11	740.8000	19	0.0000
4	0.0000	12	745.2000	20	0.0000
5	0.0000	13	702.4000	21	0.0000
6	3.5000	14	617.8000	22	0.0000
7	116.5000	15	479.5000	23	0.0000
8	303.9000	16	280.6000	24	0.0000

Table B.6 PV profile, rated 1.25 MW

Hour	Generation (kW)	Hour	Generation (kW)	Hour	Generation (kW)
1	0.0000	9	678.3100	17	71.3390
2	0.0000	10	861.1150	18	0.0000
3	0.0000	11	926.0140	19	0.0000
4	0.0000	12	931.4830	20	0.0000
5	0.0000	13	877.9420	21	0.0000
6	4.3820	14	772.2040	22	0.0000
7	145.6720	15	599.3430	23	0.0000
8	379.9020	16	350.7060	24	0.0000

Table B.7 Wind profile, rated 0.25 MW

Hour	Generation (kW)	Hour	Generation (kW)	Hour	Generation (kW)
1	138.4000	9	163.5000	17	133.2000
2	125.2000	10	154.4000	18	172.1000
3	117.3000	11	135.1000	19	190.4000
4	113.5000	12	112.7000	20	188.0000
5	115.0000	13	95.0000	21	182.1000
6	115.8000	14	90.2000	22	178.3000
7	135.4000	15	97.5000	23	162.5000
8	158.2000	16	111.5000	24	148.4000

Table B.8 Wind profile, rated 0.50 MW

Hour	Generation (kW)	Hour	Generation (kW)	Hour	Generation (kW)
1	276.8000	9	327.0000	17	266.4000
2	250.4000	10	308.8000	18	344.3000
3	234.5000	11	270.1000	19	380.8000
4	226.9000	12	225.5000	20	376.0000
5	230.0000	13	190.1000	21	364.2000
6	231.5000	14	180.4000	22	356.5000
7	270.8000	15	194.9000	23	325.0000
8	316.5000	16	223.1000	24	296.7000

Table B.9 Wind profile, rated 0.75 MW

Hour	Generation (kW)	Hour	Generation (kW)	Hour	Generation (kW)
1	415.1000	9	490.5000	17	399.5000
2	375.5000	10	463.2000	18	516.4000
3	351.8000	11	405.2000	19	571.2000
4	340.4000	12	338.2000	20	564.0000
5	345.0000	13	285.1000	21	546.3000
6	347.3000	14	270.6000	22	534.8000
7	406.2000	15	292.4000	23	487.5000
8	474.7000	16	334.6000	24	445.1000

Table B.10 Wind profile, rated 1.00 MW

Hour	Generation (kW)	Hour	Generation (kW)	Hour	Generation (kW)
1	553.5000	9	654.0000	17	532.7000
2	500.7000	10	617.6000	18	688.5000
3	469.1000	11	540.3000	19	761.7000
4	453.9000	12	450.9000	20	752.0000
5	460.1000	13	380.2000	21	728.4000
6	463.0000	14	360.9000	22	713.0000
7	541.5000	15	389.9000	23	650.0000
8	633.0000	16	446.1000	24	593.4000

Table B.11 Wind profile, rated 1.25 MW

Hour	Generation (kW)	Hour	Generation (kW)	Hour	Generation (kW)
1	691.8920	9	817.5140	17	665.8940
2	625.8990	10	771.9730	18	860.6840
3	586.3450	11	675.3310	19	952.0810
4	567.3650	12	563.6320	20	939.9630
5	575.0730	13	475.2160	21	910.5220
6	578.7850	14	451.0680	22	891.2850
7	676.9350	15	487.3670	23	812.5470
8	791.1880	16	557.6670	24	741.7850

APPENDIX C

IEEE 33-bus system test data

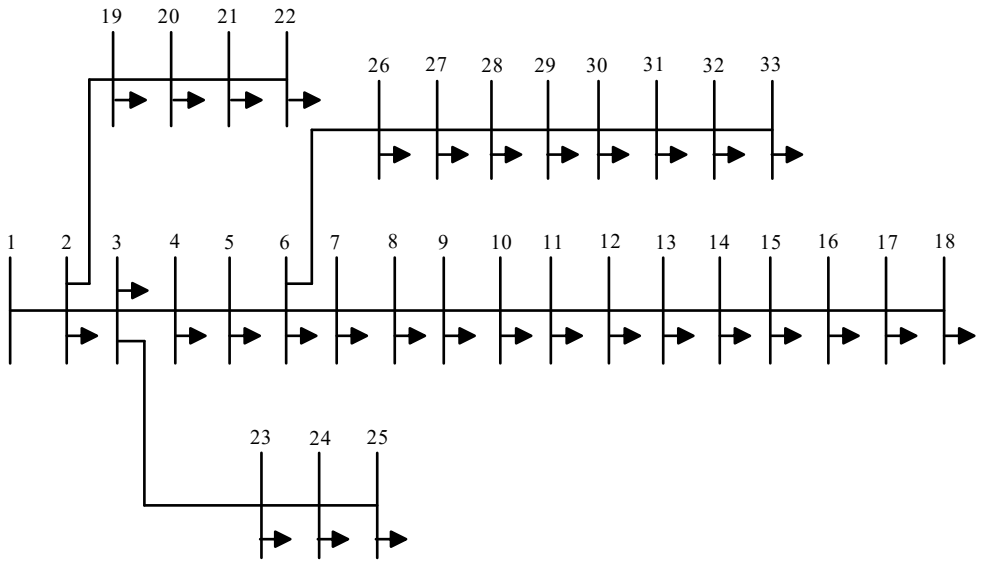

Figure C.1 IEEE 33-bus system data

Table C.1 Line parameter of IEEE 33-bus test system

From Bus	To Bus	R(p.u.)	X(p.u.)
1	2	0.0575	0.0298
2	3	0.3076	0.1567
3	4	0.2284	0.1163
4	5	0.2378	0.1211
5	6	0.5110	0.4411
6	7	0.1168	0.3861
7	8	1.0678	0.7706
8	9	0.6426	0.4617
9	10	0.6489	0.4617
10	11	0.1227	0.0406

Table C.1 Line parameter of IEEE 33-bus test system (Continued)

From Bus	To Bus	R(p.u.)	X(p.u.)
11	12	0.2336	0.0772
12	13	0.9159	0.7206
13	14	0.3379	0.4448
14	15	0.3687	0.3282
15	16	0.4656	0.3400
16	17	0.8042	1.0738
17	18	0.4567	0.3581
2	19	0.1023	0.0976
19	20	0.9385	0.8457
20	21	0.2555	0.2985
21	22	0.4423	0.5848
3	23	0.2815	0.1924
23	24	0.5603	0.4424
24	25	0.5590	0.4374
6	26	0.1267	0.0645
26	27	0.1773	0.0903
27	28	0.6607	0.5826
28	29	0.5018	0.4371
29	30	0.3166	0.1613
30	31	0.6080	0.6008
31	32	0.1937	0.2258
32	33	0.2128	0.3308

Table C.2 Power parameter of IEEE 33-bus test system

Bus	Type	P(MW)	Q(MVar)
1	slack	0.0000	0.0000
2	PQ	0.1000	0.0600
3	PQ	0.0900	0.0400
4	PQ	0.1200	0.0800
5	PQ	0.0600	0.0300
6	PQ	0.0600	0.0200
7	PQ	0.2000	0.1000
8	PQ	0.2000	0.1000
9	PQ	0.0600	0.0200
10	PQ	0.0600	0.0200
11	PQ	0.0450	0.0300
12	PQ	0.0600	0.0350
13	PQ	0.0600	0.0350
14	PQ	0.1200	0.0800
15	PQ	0.0600	0.0100
16	PQ	0.0600	0.0200
17	PQ	0.0600	0.0200
18	PQ	0.0900	0.0400
19	PQ	0.0900	0.0400
20	PQ	0.0900	0.0400
21	PQ	0.0900	0.0400
22	PQ	0.0900	0.0400
23	PQ	0.0900	0.0500
24	PQ	0.4200	0.2000
25	PQ	0.4200	0.2000
26	PQ	0.0600	0.0250
27	PQ	0.0600	0.0250
28	PQ	0.0600	0.0200

Table C.2 Power parameter of IEEE 33-bus test system (Continued)

Bus	Type	P(MW)	Q(MVar)
29	PQ	0.1200	0.0700
30	PQ	0.2000	0.6000
31	PQ	0.1500	0.0700
32	PQ	0.2100	0.1000
33	PQ	0.0600	0.0400

APPENDIX D

IEEE 69-bus system test data

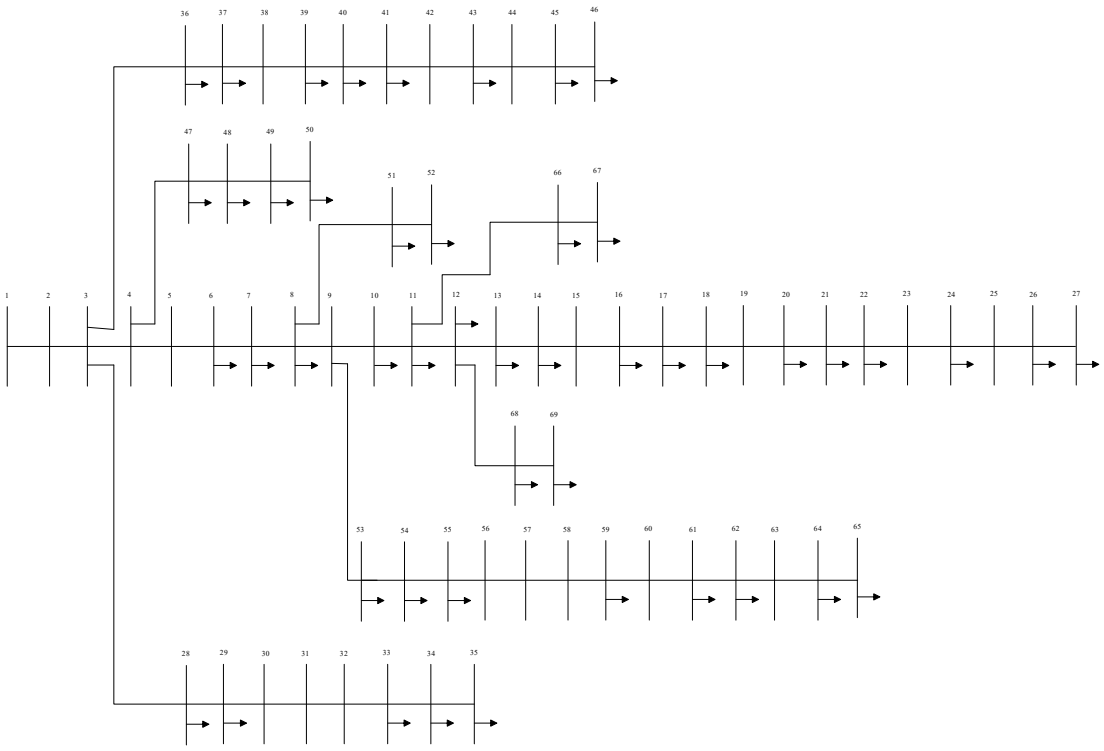

Figure D.1 IEEE 69-bus system data

Table D.1 Line parameter of IEEE 69-bus test system

From Bus	To Bus	R(p.u.)	X(p.u.)
1	2	3.12e-05	7.487e-05
2	3	3.12e-05	7.487e-05
3	4	9.359e-05	0.00022461
4	5	0.00156605	0.00183434
5	6	0.02283567	0.01162997
6	7	0.02377779	0.01211039
7	8	0.00575259	0.00293245

Table D.1 Line parameter of IEEE 69-bus test system (Continued)

From Bus	To Bus	R(p.u.)	X(p.u.)
8	9	0.00307595	0.00156605
9	10	0.05109948	0.01688966
10	11	0.01167988	0.0038621
11	12	0.04438605	0.01466848
12	13	0.0642643	0.02121346
13	14	0.0651378	0.02152542
14	15	0.0660113	0.02181243
15	16	0.01226637	0.00405551
16	17	0.02335976	0.0077242
17	18	0.00029324	9.983e-05
18	19	0.02043979	0.00675711
19	20	0.01313987	0.00434252
20	21	0.02131329	0.00704412
21	22	0.0008735	0.00028701
22	23	0.00992665	0.00328185
23	24	0.02160653	0.00714394
24	25	0.04671953	0.01544215
25	26	0.01927305	0.00637028
26	27	0.01080639	0.00356885
27	28	0.00027453	0.00067384
28	29	0.00399312	0.00976443
29	30	0.02481975	0.00820462
30	31	0.00437996	0.00144751
31	32	0.02189978	0.00723753
32	33	0.05234733	0.01756974
33	34	0.10656644	0.03522682
34	35	0.09196659	0.03040388
35	36	0.00027453	0.00067384

Table D.1 Line parameter of IEEE 69-bus test system (Continued)

From Bus	To Bus	R(p.u.)	X(p.u.)
36	37	0.00399312	0.00976443
37	38	0.00656993	0.00767428
38	39	0.00189673	0.00221493
39	40	0.00011231	0.00013102
40	41	0.04544048	0.0530898
41	42	0.01934168	0.02260481
42	43	0.00255809	0.00298236
43	44	0.00057401	0.00072375
44	45	0.00679455	0.00856649
45	46	5.615e-05	7.487e-05
46	47	0.00021213	0.0005241
47	48	0.0053096	0.01299636
48	49	0.01808135	0.04424254
49	50	0.00512867	0.01254714
50	51	0.00579003	0.00295117
51	52	0.02070808	0.00695053
52	53	0.0108563	0.00552798
53	54	0.01266568	0.00645139
54	55	0.01773196	0.0090282
55	56	0.01755102	0.00894085
56	57	0.09920412	0.03329889
57	58	0.04889702	0.01640924
58	59	0.01897981	0.00627669
59	60	0.02408976	0.0073124
60	61	0.03166421	0.01612847
61	62	0.00607703	0.00309467
62	63	0.00904692	0.00460457
63	64	0.04432989	0.02257986

Table D.1 Line parameter of IEEE 69-bus test system (Continued)

From Bus	To Bus	R(p.u.)	X(p.u.)
64	65	0.06495062	0.03308052
65	66	0.01255338	0.00381218
66	67	0.00029324	8.735e-05
67	68	0.04613304	0.01524873
68	69	0.00029324	9.983e-05

Table D.2 Power parameter of IEEE 69-bus test system

Bus	Type	P(MW)	Q(Var)
1	slack	0.0000	0.0000
2	PQ	0.0000	0.0000
3	PQ	0.0000	0.0000
4	PQ	0.0000	0.0000
5	PQ	0.0000	0.0000
6	PQ	0.0026	0.0022
7	PQ	0.0404	0.0300
8	PQ	0.0750	0.0540
9	PQ	0.0300	0.0220
10	PQ	0.0280	0.0190
11	PQ	0.1450	0.1040
12	PQ	0.1450	0.1040
13	PQ	0.0080	0.0055
14	PQ	0.0080	0.0055
15	PQ	0.0000	0.0000
16	PQ	0.0455	0.0300
17	PQ	0.0600	0.0350
18	PQ	0.0600	0.0350
19	PQ	0.0000	0.0000
20	PQ	0.0010	0.0006

Table D.2 Power parameter of IEEE 69-bus test system (Continued)

Bus	Type	P(MW)	Q(Var)
21	PQ	0.1140	0.0810
22	PQ	0.0053	0.0035
23	PQ	0.0000	0.0000
24	PQ	0.0280	0.0200
25	PQ	0.0000	0.0000
26	PQ	0.0140	0.0100
27	PQ	0.0140	0.0100
28	PQ	0.0260	0.0186
29	PQ	0.0260	0.0186
30	PQ	0.0000	0.0000
31	PQ	0.0000	0.0000
32	PQ	0.0000	0.0000
33	PQ	0.0140	0.0100
34	PQ	0.0195	0.0140
35	PQ	0.0060	0.0040
36	PQ	0.0260	0.0186
37	PQ	0.0260	0.0186
38	PQ	0.0000	0.0000
39	PQ	0.0240	0.0170
40	PQ	0.0240	0.0170
41	PQ	0.0012	0.0010
42	PQ	0.0000	0.0000
43	PQ	0.0060	0.0043
44	PQ	0.0000	0.0000
45	PQ	0.0392	0.0263
46	PQ	0.0392	0.0263
47	PQ	0.0000	0.0000
48	PQ	0.0790	0.0564

Table D.2 Power parameter of IEEE 69-bus test system (Continued)

Bus	Type	P(MW)	Q(Var)
49	PQ	0.3847	0.2745
50	PQ	0.3847	0.2745
51	PQ	0.0405	0.0283
52	PQ	0.0036	0.0027
53	PQ	0.0043	0.0035
54	PQ	0.0264	0.0190
55	PQ	0.0240	0.0172
56	PQ	0.0000	0.0000
57	PQ	0.0000	0.0000
58	PQ	0.0000	0.0000
59	PQ	0.1000	0.0720
60	PQ	0.0000	0.0000
61	PQ	1.2440	0.8880
62	PQ	0.0320	0.0230
63	PQ	0.0000	0.0000
64	PQ	0.2270	0.1620
65	PQ	0.0590	0.0420
66	PQ	0.0180	0.0130
67	PQ	0.0180	0.0130
68	PQ	0.0280	0.0200
69	PQ	0.0280	0.0200

APPENDIX E

List of publications

T. Phimtakhob and K. Chayakulkheeree (2024), Microgrid Voltage Stability Indices Improvement Using Particle Swarm Optimization., 2024 International Electrical Engineering Congress (iEECON2024), Pattaya, Thailand.

T. Phimtakhob and K. Chayakulkheeree (2024), Voltage Deviation Improvement in Active Distribution Network Using Battery Energy Storage System Optimal Voltage Droop Control., GMSARN International Journal.

2024 International Electrical Engineering Congress (iEECON 2024)
March 6-8, 2024, Pattaya Chonburi, THAILAND

Microgrid Voltage Stability Indices Improvement Using Particle Swarm Optimization

Thanarat Phimtakhob, Keerati Chayakulkheeree
School of electrical engineering
Institute of Engineering
Suranaree University of Technology
Nakhon Ratchasima, Thailand
Thanarat.ptk@gmail.com, keerati.ch@sut.ac.th

***Abstract*— This paper provides a strategy for improving microgrid voltage stability indices (VSI) using particle swarm optimization (PSO). The L-index value is used to assess the weak bus of the system. The IEEE 33-bus system is used for evaluating the proposed method, including four cases as follows; the IEEE 33-bus base case, the IEEE 33-bus with L-index improvement, the IEEE 33-bus as microgrid (MG), and the modified IEEE 33-bus as microgrid with L-index improvement. For VSI improvement, PSO is utilized to determine the generator bus voltages for minimizing the L-index. The proposed method can successfully minimize the L-index for both conventional distribution networks and MG systems, from the simulation results.**

Keywords— Voltage Stability, weak bus, L-index, PV-curve, optimization

I. INTRODUCTION

The electrical system operation has changed significantly in recent years. This is due to an increment in distributed energy resources (DERs) that drives the distribution networks to the active distribution network (ADNs) or microgrids (MGs) [1]. An MG is a small system that combines multiple generators and loads. In the MG system, most of the energy used is from Renewable energy resources include solar cells, wind power, and so on [2]. MG operation can help the system in terms of reliability by reducing the cost of producing electricity [3]. However, maintaining stability in the MG system is critical for both voltage and frequency stabilities. A microgrid system's operating mode has a significant impact on its performance and dependability. MG operating modes are classified into two types: grid-connected and isolated. In grid-connected mode, the MG system connects to the main grid and can exchange power and energy with it. In isolated mode, the microgrid is detached from the main grid, and supplying the load by its own distributed energy resources. MG systems may face abnormal conditions while transitioning from grid-connected to isolated mode. Specifically in terms of voltage stability. As a result, having the right tools and methodologies is critical for ensuring voltage stability in isolated MG systems [4]. As a result, rigorous monitoring and oversight are required to ensure that the electrical system is as stable as feasible [5]. The Countries that experienced voltage collapse and long-term power outages are occurs include Bangladesh, the United States, Japan, and Canada [6-7]. From history, it can be observed that no matter how complex the system that the voltage collapse can happen.

Voltage stability is a fundamental feature of power system functioning, and it refers to an electrical network's ability to maintain a stable and appropriate voltage profile under various operating conditions [8]. Voltage is a basic element in an electric power system that must be controlled within specific parameters to ensure the dependable and secure delivery of electricity to users. Voltage instability occurs when voltage levels in the electrical grid deviate significantly from their nominal values, which can cause a variety of problems such as voltage sags, voltage collapses, and even blackouts. The overall stability and dependability of the electrical system may be significantly impacted by this [9].

The voltage stability index (VSI), provides a sufficiently precise and more pragmatic approach to assessment, enabling the representation of stability analysis in a straightforward manner [10]. There are many indicators proposed to forecast or detect voltage collapse in the power system. Phanikumar and Kanta Rao use the model analysis method and sensitive method to observe the stability of the power system [11]. Reference [12] employs the fast voltage stability index to detect weak lines and weak buses. In addition, reference [13] determines the weak bus using the L-index. Vadivelu shows how to calculate the maximum load capacity of an electrical system using a line voltage stability index, such as the fast voltage stability index [14]. Salama and Vokony examine and analyze several voltage stability indexes, including the line index and bus index, presenting benefits, drawbacks, and calculation formulas [15].

This paper uses the L-index values to determine which bus in the system is the weakest. The voltage stability improves with a lower L-index value. Each load bus contains its own L-index based on the power network admittance characteristic. By using particle swarm optimization (PSO), the optimal generator voltage that minimizes the L-index value can be obtained. Finally, PV curves for the weakest buses of the system are determined to evaluate the system performance.

The paper is structured as follows: Section 1 addresses an introduction Section 2 illustrates the L-index computation Section 3 contains the proposed technique Section 4 provides and discusses the simulation results and Section 5 gives the conclusion.

II. L-INDEX

In this study, the L-index is used to predict the incidence of electrical collapse and it is a simple technique for calculating and identifying weak busses. therefore, it is a tool that may be improved to increase system stability. Using the following equation:

2024 12th International Electrical Engineering Congress (iEECON) | 979-8-3503-8359-1/24/$31.00 ©2024 IEEE | DOI: 10.1109/IEECON60677.2024.10537938

2024 International Electrical Engineering Congress (iEECON 2024)
March 6-8, 2024, Pattaya Chonburi, THAILAND

Before determining the indicator L, evaluate the current flow in the system using the following equation:

$$I_{bus} = Y_{bus} V_{bus} \tag{1}$$

And because the system includes multiple buses, we can consider them in the matrix.

$$\begin{bmatrix} \mathbf{I^G} \\ \mathbf{I^L} \end{bmatrix} = \begin{bmatrix} \mathbf{Y^{GG}} & \mathbf{Y^{GL}} \\ \mathbf{Y^{LG}} & \mathbf{Y^{LL}} \end{bmatrix} \begin{bmatrix} \mathbf{V^G} \\ \mathbf{V_L} \end{bmatrix} \tag{2}$$

$$\mathbf{I^G} = \mathbf{Y^{GG}V^G} + \mathbf{Y^{GL}V^L} \tag{3}$$

$$\mathbf{I^L} = \mathbf{Y^{LG}V^G} + \mathbf{Y^{LL}V^L} \tag{4}$$

Where $\mathbf{I^G}$ is current at generator bus, $\mathbf{I^L}$ is current at load bus, $\mathbf{V^G}$ is voltage at generator bus and $\mathbf{V^L}$ is voltage at load bus After some mathematical manipulation, equation (2) can be written as equations (5)–(7).

$$\mathbf{V^L} = \mathbf{[Y^{LL}]^{-1}I^L} - \mathbf{[Y^{LL}]^{-1}Y^{LG}V^G} \tag{5}$$

$$\mathbf{I^G} = \mathbf{Y^{GL}[Y^{LL}]^{-1}I^L} + (\mathbf{Y^{GG}} - \mathbf{Y^{GL}[Y^{LL}]^{-1}Y^{LG}})\mathbf{V^G} \tag{6}$$

Equations (5) and (6) in matrix form

$$\begin{bmatrix} \mathbf{V^L} \\ \mathbf{I^G} \end{bmatrix} = \begin{bmatrix} \mathbf{[Y^{LL}]^{-1}} & -\mathbf{[Y^{LL}]^{-1}Y^{LG}} \\ \mathbf{Y^{GL}[Y^{LL}]^{-1}} & \mathbf{Y^{GG}} - \mathbf{Y^{GL}[Y^{LL}]^{-1}Y^{LG}} \end{bmatrix} \begin{bmatrix} \mathbf{I^L} \\ \mathbf{V^G} \end{bmatrix} \tag{7}$$

Rearranging the above matrix we get,

$$\begin{bmatrix} \mathbf{V^L} \\ \mathbf{I^G} \end{bmatrix} = \begin{bmatrix} \mathbf{Z^{LL}} & \mathbf{F^{LG}} \\ \mathbf{K_{GL}} & \mathbf{Y^{GG}} \end{bmatrix} \begin{bmatrix} \mathbf{I^L} \\ \mathbf{V^G} \end{bmatrix} \tag{8}$$

$$\mathbf{F_{LG}} = -\mathbf{Y_{LL}}^{-1}\mathbf{Y_{LG}} \tag{9}$$

$$L_j = \left| 1 - \sum_{i=1}^{i=g} F_{ij} \frac{V_i}{V_j} \right| \tag{10}$$

Where,

g is the total number of generators,

L_j is the L-index value of the bus,

V_i is the voltage at the generator bus,

V_j is the voltage at the load bus j,

F_{ij} is the element of the $\mathbf{F_{LG}}$ matrix obtained by (9) [16].

$\mathbf{Y_{LL}}$ and $\mathbf{Y_{LG}}$ are the submatrix of $\mathbf{Y_{bus}}$ that rearranged to represent the correlation between load buses and between load and generator buses, respectively.

Prior to computing the L-Index, the voltage values for each system bus and Y-bus must be known. These are computed using the Newton-Raphson load flow (NRLF) method. Next, the matrix $\mathbf{F_{LG}}$ is obtained by converting it from Y-bus. Then (10) is used in order to obtain the value of the L-Index. Note that the L-Index holds the value for only load buses. Furthermore, if the L-Index value is closest to 1, it indicates that the bus is the weakest bus and could potentially cause the voltage collapse to the system. Conversely, the most powerful bus is indicated by the L-Index value closest to 0.

III. Voltage Stability Improvement Using PSO

PSO is a well-known metaheuristic approach inspired by birds flocking to find food. It iteratively searches the solution space by adjusting particle positions until it discovers the best-known and global best positions, with the goal of finding an optimal solution. as well as velocity updates [17].

PSO emerges as a potential method for improving voltage stability in microgrid systems. It accomplishes this by determining the appropriate generator bus voltage to reduce the L-index, which is a critical indicator of the voltage stability margin. PSO's intrinsic features, such as simplicity, computational efficiency, and adaptability, make it ideal for use in this case.

The objective function or fitness function to minimize the L-index value of the weakest bus can be written as,

$$\text{minimize} \qquad \text{f}(\text{x}_i^t) = \max\{\text{L-index}\}, \tag{11}$$

and the following equations are used to compute velocity and position,

$$v_i^{t+1} = wv_i^t + c_1 r_1 (pBest_i^t - x_i^t) + c_2 r_2 (gBest_i^t - x_i^t), \tag{12}$$

$$x_i^{t+1} = x_i^t + v_i^t. \tag{13}$$

Where,

$pBest$ is the best value of each particle, where $pBest$ used to update the population,

$gBest$ is the best value of all particles,

t and $t+1$ is the iteration,

v_i is the velocity for particle i,

c_1 and c_2 is a constant numbers,

r_1 and r_2 is a random parameters,

w is inertial weight, and

x_i is the population of particles that represent the generator's voltage values. The lowest and top limits of the generator's voltage are 0.9 and 1.1, respectively. The proposed PSO based VSI improvement computational procedure is illustrated in Fig. 1.

Another crucial instrument for assessing the stability of a system is the PV curve. PV curve is obtained by step-wise increasing the real power loading of the selected bus and calculating the load flow to obtain the bus voltage. The computational step is repeated until the load flow is infeasible. Then, the plot between the bus real power load and the bus voltage or PV curve can represent the voltage collapse characteristic of the system [18].

2024 International Electrical Engineering Congress (iEECON 2024)
March 6-8, 2024, Pattaya Chonburi, THAILAND

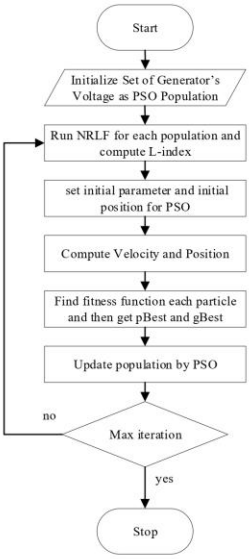

Fig. 1. Computation Procedure

IV. RESULTS AND DISCUSSION

This section displays the results of the suggested approach on the IEEE 33-bus system. It is separated into four cases, as shown below.

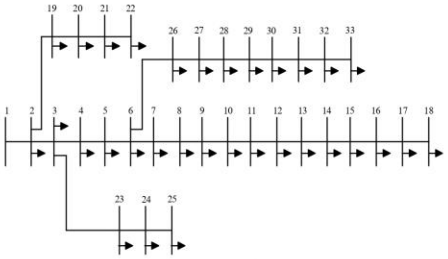

Fig. 2. IEEE 33-bus system

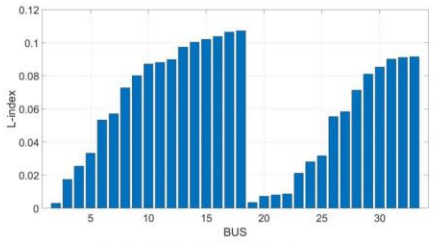

Fig. 3. L-index of IEEE 33-bus base case

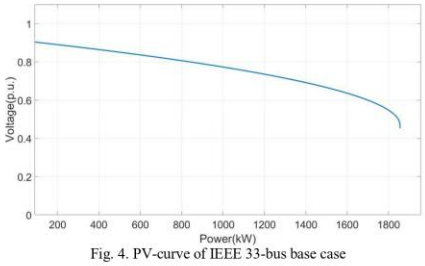

Fig. 4. PV-curve of IEEE 33-bus base case

A. *IEEE 33-bus base case*

As illustrated in Fig. 2, the base case IEEE 33-bus system consists of one slack bus and 32 load buses, with the voltage value at the slack bus set to 1 p.u.

Figure 3 depicts the L-Index values of each bus. Bus 18 provides the most L-Index value, so it is the weak bus. Meanwhile, bus 2 resulted in lower L-Index value and, therefore, it is a strong bus. Bus 18 has the highest possibility of voltage collapse of this system. Figure 4 shows the PV-curve of bus 18, where the voltage is collapsed at 1854.9 kW of power leading.

B. *IEEE 33-bus with L-index improvement*

With the proposed method, the optimal value for the generator voltage at the slack bus is 1.1 p.u.

Figure 5 shows that in this optimized system, the L-index value is reduced. Bus 18 is still a weak bus, as is Bus 2, which is still a strong bus. However, when compared with the previous case, the L-index value is lower. Figure 6 shows the PV curve of the optimized system. The maximum loading capability of bus 18 is increased to 2355.3 kW.

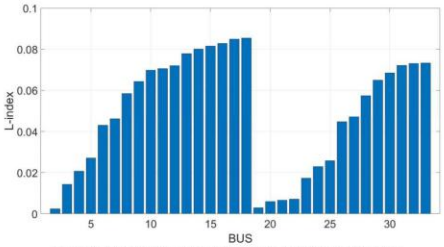

Fig. 5. L-index of IEEE 33-bus with L-index improvement

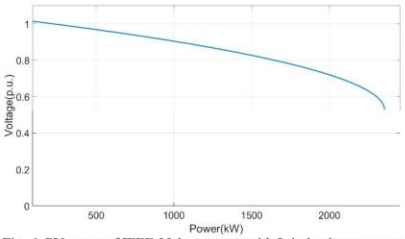

Fig. 6. PV-curve of IEEE 33-bus system with L-index improvement

2024 International Electrical Engineering Congress (iEECON 2024)
March 6-8, 2024, Pattaya Chonburi, THAILAND

C. IEEE 33-bus Modified

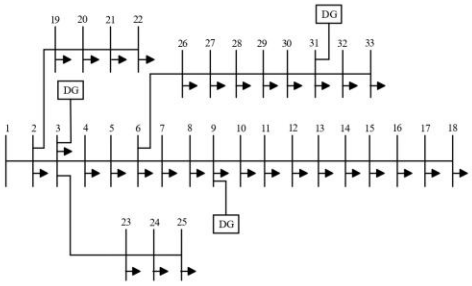

Fig. 7. Modified IEEE 33-bus system

In this case, the IEEE 33-bus system is modified by adding three distributed generators (DGs) at buses 3, 9, and 31 with power generators of 1.9 MW, 0.95 MW, and 1.69 MW, respectively [19]. Bus 1 is disconnected from the main power grid for the MGs case study. The values of the voltages at all generator buses are set to 1 p.u. Bus 3 is set to slack bus.

Figure 8 shows the L-index of the modified IEEE 33-bus, similarly Bus 18 is a weaker bus, while bus 2 is a stronger bus. As observed, the weak bus is the farthest bus from the power sources. On the other hand, the strong bus is the nearest to the power sources. Figure 9 shows the PV-curve of bus 18, The maximum loading capability is 3852.9 kW.

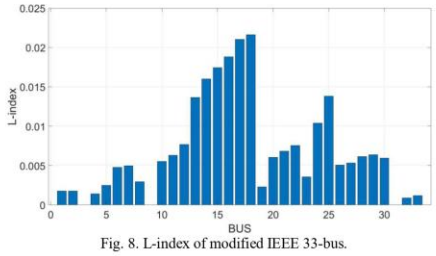

Fig. 8. L-index of modified IEEE 33-bus.

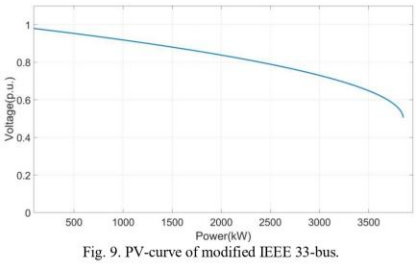

Fig. 9. PV-curve of modified IEEE 33-bus.

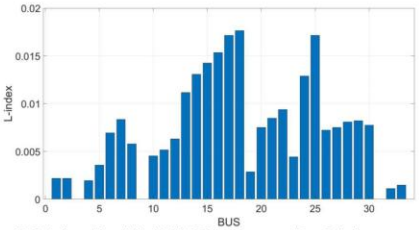

Fig. 10. L-index of modified IEEE 33-bus system with L-index improvement.

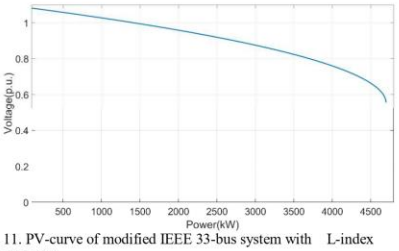

Fig. 11. PV-curve of modified IEEE 33-bus system with L-index improvement.

D. Modified IEEE 33-bus system with L-index improvement.

Figure 10 depicts the L-index values for each bus in the modified IEEE 33-bus system. The L-index value has decreased significantly when compared to previous cases. Bus 18 is a weak bus, while Bus 2 is a strong bus.

Figure 11 shows the PV curve of the modified IEEE 33-bus system with L-index improvement. It is found that in this case, the maximum loading is increased to 4698.9 kW, indicating that the system can handle a higher loading level. this system is very stable.

From Table 1, it is found that for systems voltage stability has been improving, with a reduction of the L-Index values. This reduction in L-Index values significantly improves system stability by the optimization process. The L-index values that are not presented in the table are those at the PV bus, where the L-index computation solely applies to bus loads. The PV buses are IEEE 33-bus base case system bus 1 and IEEE 33-bus Modified system buses 3, 9, and 31. In assessing the system stability, bus 18 emerges with the highest L-index value. This observation implies that bus 18 is the least reliable and possesses the greatest potential to induce system instability. Consequently, to uphold system stability, particular attention should be directed towards bus number 18 within the system. Addressing or optimizing the conditions associated with Bus 18 becomes critical in preserving the overall stability of the IEEE 33-bus system.

The PV curves also show that the modified IEEE 33-bus system is the most stable, as it can handle the highest load compared to other cases.

TABLE I. COMPARING L-INDEX VALUE

BUS	L-index			
	IEEE 33-bus base case	***IEEE 33-bus with L-index improvement***	***IEEE 33-bus Modified***	***IEEE 33-bus Modified with L-index improvement***
1	-	-	0.001772	0.00219
2	0.003004	0.002454	0.001772	0.00219
3	0.017498	0.014244	-	-
4	0.025411	0.020637	0.001415	0.00195
5	0.033364	0.02704	0.002505	0.003562
6	0.053276	0.042984	0.004789	0.00692
7	0.057172	0.046085	0.004961	0.008352
8	0.072771	0.05846	0.002968	0.005789
9	0.080183	0.064309	-	-
10	0.087129	0.069775	0.001415	0.00195
11	0.088143	0.070571	0.002505	0.003562
12	0.089917	0.071964	0.004789	0.00692
13	0.097415	0.077838	0.004961	0.008352
14	0.100304	0.080097	0.002968	0.005789
15	0.102096	0.081497	0.017461	0.014241
16	0.103813	0.082837	0.018828	0.015352
17	0.10646	0.084901	0.021021	0.017133
18	0.107227	0.085498	0.021628	0.017626
19	0.003527	0.002885	0.002313	0.00286
20	0.00723	0.005937	0.006068	0.007512
21	0.007993	0.006564	0.006841	0.008471
22	0.008698	0.007145	0.007558	0.009361
23	0.021172	0.017244	0.003574	0.004428
24	0.028149	0.022928	0.01038	0.012882
25	0.031696	0.025812	0.013806	0.017149
26	0.055454	0.044721	0.005074	0.007212
27	0.058377	0.047049	0.005345	0.00751
28	0.071425	0.057412	0.006137	0.008081
29	0.081028	0.065007	0.006387	0.008205
30	0.085367	0.068429	0.00597	0.007742
31	0.090123	0.072171	-	-
32	0.091174	0.072997	0.000907	0.00112
33	0.0915	0.073253	0.001192	0.001471

V. CONCLUSION

The proposed PSO based VSI improvement was tested with the IEEE 33-bus system, under the conventional distribution system, and modified to the MG system. The primary objective is to identify the bus exerting the most significant influence on system instability, utilizing the L-index. The results demonstrated that the proposed method could reduce the L-index of the system's weakest bus., leading to voltage stability improvement and loading capability increment. In future work, additional factors of voltage regulation could be studied using data from the reliable L-index as a consistent bus selection criterion to maintain system stability.

ACKNOWLEDGMENT

We want to offer our profound gratitude to Suranaree University of Technology for their invaluable assistance with scholarships and resources during the period of this research project. Their vast knowledge and unwavering support were critical in bringing this study to a successful conclusion.

REFERENCES

[1] I. G. Adebayo and Y. Sun, "A comparison of voltage stability indices for critical node identification in a power system," *2021 International Conference on Sustainable Energy and Future Electric Transportation (SEFET)*, Jan. 2021.

[2] L. Jimin and N. Ming, "Overview on microgrid research and development," in *Communications in computer and information science*, 2010, pp. 161–168.

[3] A. Kumar, M. Z. U. Khan, and D. M. A. Hussain, "Microgrids Technology: A Review paper," *Gyancity Journal of Electronics and Computer Science*, vol. 3, no. 1, pp. 11–20, Mar. 2018.

[4] R. Kljajić, P. Marić, H. Glavaš, and M. Žnidarec, "Microgrid Stability: A Review on Voltage and Frequency Stability," *2020 IEEE 3rd International Conference and Workshop in Óbuda on Electrical and Power Engineering (CANDO-EPE)*, Nov. 2020.

[5] Y. A. Mashhadany, A. K. Abbas, and S. Algburi, "Study and analysis of power system stability based on FACT Controller System," *Indonesian Journal of Electrical Engineering and Informatics*, vol. 10, no. 2, Jun. 2022.

[6] R. Gadal, A. Oukennou, F. Elmariami, A. Belfqih, and N. Agouzoul, "Voltage Stability Assessment and Control Using Indices and FACTS: A Comparative review," *Journal of Electrical and Computer Engineering*, vol. 2023, pp. 1–18, Aug. 2023.

[7] C. Dondariya, D.K. Sakravdia, "A comprehensive investigation on voltage stability indices for distributed generation placement and sizing," 2021.

[8] Ieee Committee Report, Voltage Stability of Power Systems: Concepts Analytical Tools and Industry Experience, Springer, Berlin, Germany, 1990.

[9] H. H. Alhelou, M. E. Hamedani-Golshan, T. C. Njenda, and P. Siano, "A survey on power system blackout and cascading Events: Research Motivations and challenges," *Energies*, vol. 12, no. 4, p. 682, Feb. 2019.

[10] E. Z. Yahia, M. Elsherif, and M. Zaggout, "Detection of proximity to voltage collapse byUsing 1 Ã¢ÂÂIndex," *International Journal of Innovative Research in Science, Engineering and Technology*, vol. 4, no. 3, pp. 1755–1765, Jul. 2015.

[11] M. S. V. Phanikumar and P. Rao, "Comparison of voltage stability and loss reduction by modal analysis and sensitivity methods," vol. 16, pp. 183-188, 01/01 2016.

[12] I. G. Adebayo, A. A. Jimoh, and A. A. Yusuff, "Detection of weak bus through Fast Voltage Stability index and inherent structural characteristics of power system," *2015 4th International Conference on Electric Power and Energy Conversion Systems (EPECS)*, Nov. 2015.

[13] A. K. Karn, S. Hameed, and M. Sarfraz, "Identification of Strong and Weak Bus and Optimal Bus Coupling by L —Index Coefficients For Voltage Regulation in Power System," *2023 International Conference on Power, Instrumentation, Energy and Control (PIECON)*, Feb. 2023.

[14] A. K. Sharma, A. Saxena, R. Tiwari, and R. Scholar, "Maximum Loadability Estimation for Weak Bus Identification using Line Stability Indices," *ResearchGate*, Jan. 2017.

[15] H. S. Salama and I. Vokony, "Voltage stability indices–A comparison and a review," *Computers & Electrical Engineering*, vol. 98, p. 107743, Mar. 2022.

[16] P. Kessel and H. Glavitsch, "Estimating the voltage stability of a power system," *IEEE Transactions on Power Delivery*, vol. 1, no. 3, pp. 346–354, Jan. 1986.

[17] J. Kennedy and R. C. Eberhart, "Particle swarm optimization," *Proceedings of ICNN'95 - International Conference on Neural Networks*, Nov. 2002.

[18] T. Van Cutsem and C. Vournas, Voltage stability of electric power systems. Springer, 1998.

[19] M. V. Kirthiga and S. A. Daniel, "Computational techniques for autonomous microgrid load flow analysis," *ISRN Power Engineering*, vol. 2014, pp. 1–12, May 2014.

Voltage Deviation Improvement in Active Distribution Network Using Battery Energy Storage System Optimal Voltage Droop Control

Thanarat Phimtakhob [1] and Keerati Chayakulkeeree [1,*]

ARTICLE INFO

Article history:
Received:
Revised:
Accepted:

Keywords:
Battery Energy Storage
Voltage Regulation
Voltage Deviation
Adaptive Droop Control
Particle Swarm Optimization

ABSTRACT

This work proposes the implementation of battery energy storage system (BESS) management for voltage regulation in the active distribution network (ADN). The primary goal is to minimize the overall voltage deviation of all buses in the power system. Adaptive droop control is employed to regulate BESS and optimize the efficiency of battery operation. In order to enhance the performance of the battery energy storage system, the study employs particle swarm optimization (PSO) to identify the most effective control parameters. To validate the efficacy of the proposed methodology, its performance is examined utilizing an IEEE 33-bus distribution system by testing scenarios both with and without renewable energy sources such as photovoltaic panels and wind turbines. The results demonstrate that the approach extensively decreases the voltage deviation in three scenarios, including with/without BESS. The optimization of BESS management can effectively confine the voltage within the established range of 0.95 – 1.05 and minimize the voltage deviation of all buses to a minimum of 0.0385 p.u. Consequently, this leads to an enhancement in the voltage profile, power quality, and system dependability.

1. INTRODUCTION

Voltage stability in the electrical system is extremely important and must be prioritized. In modern distribution network (DN), renewable energy is currently increasing rapidly, due to the increase in photovoltaic (PV) and wind power. Therefore, many DNs have been transformed into active distribution network (ADNs). The main issue with renewable energy is the discontinuity of the energy that can be generated [1]. These are the challenges that make ADN voltage control more difficult. One of the key indices for voltage stability is voltage deviation (VD). It measures the difference of voltage value from the nominal value. If it exceeds the specified standard, it may have an impact on system efficiency or even cause damage to electrical equipment [2-4]. As a result, many tools have been developed over time to help maintain voltage stability, including transformer load tap changes, shunt capacitor banks, and STATCOM [5]. These tools help to enhance the stability of the electrical system. For example, Sarithumu et al. [6] developed a strategy to regulate voltage in networks with a high level of renewable energy penetration, making the use of traditional tools or methods ineffective, Thus, a technique utilizing on-load tap changer voltage regulation was devised for voltage control. According to Abedini et al. [7], shunt capacitor banks can give a good solution for voltage profile problems in power systems by delivering reactive power to the system, but they still have the problem of transient signals, which might impact sensitive devices. According to Gurav and Mittal [8], STATCOM can supply fast reactive power, but it is not always effective due to the trial-and-error control strategy in controller configuration. Similarly, Xu and Li [9] claimed that classical STATCOM control should not be used in engineering or the real world, despite the fact that it has the advantage of providing fast reactive power.

As mentioned, most conventional devices still have several limitations compared to battery energy storage system (BESS), such as fast response, which can bring more benefits than just voltage regulation. As a result, the usage of BESS is intriguing and has great promise for controlling voltage in power systems and resolving VD issues [10]. BESS has several operating functions, for example, energy arbitrage that provides lowering electricity cost, peak shaving for reducing the peak demand, and even store the excess energy for utilizing in the shortage period [11]. In addition, BESS can also regulate the system frequency and voltage [12]. However, for batteries to function optimally, they must be properly managed or controlled. Several research studies have explored battery management strategies. Mohammed et al. [13] focus on improving the sizing of a stand-alone hybrid energy system that consists of three components: PV, diesel generator, and BESS. Saini and Gidwani [14] use BESS as an alternative load for charging and discharging. The objective is to minimize

[1] *School of Electrical Engineering, Institute of Engineering, Suranaree University of Technology, Nakhon Ratchasima, Thailand*
**Corresponding author:* Email: keerati.ch@sut.ac.th

yearly energy losses, alleviate reverse power flow, and resolve overvoltage challenges in an IEEE 69-bus system integrated with PV. Tamrakar et al. [15] suggest employing BESS to replace outdated equipment like on-load tap changer capacitor banks. To improve system dependability, Zhang et al. [16] presents a multi-agent system-based control approach for energy storage and PV inverters. Alam et al. [17] presents a novel charge and discharge control scheme that takes into account the status of the charging current. Considering the impact of solar cells in the system in terms of energy efficiency, the storage is utilized to catch the extra energy produced by PV during the PV peak and store it for peak load support. Tandon et al. [18] discovered the optimal allocation of BESS to increase system performance while taking into account load volatility, renewable energy sources, and network constraints. Alzahrani et al. [19] used BESS in a system with high PV deployment to explore system loss and power quality issues, employing a genetic algorithm-based placement methodology. Wang et al. [20] proposed employing BESS to address voltage instability issues in low-voltage grids with high rooftop PV penetration, considering the state of charge (SoC). Rouzbehi et al. [21] proposed a generalized voltage droop (GVD) control approach to address the voltage rise issue. GVD operates in three modes: fixed voltage control, fixed active power control, and traditional voltage droop control (VDC), all of which can be changed using the GVD characteristic of a voltage regulation inverter. Zeraati et al. [22] employed BESS to handle various voltage difficulties, such as voltage rise, and presented a collaboration between a local droop-based control approach for battery installation size and a distributed control system to manage SoC performance to prevent battery saturation. Chen et al. [23] suggested a fuzzy logic-based adaptive droop controller to alter the droop coefficient, resulting in a compromise between DC. Jamreon and Sirisukprasert [24] presented a voltage control technique integrating battery energy storage with SoC management. The battery control employs adaptive droop control as a power supply controller, as well as self-learning particle swarm optimization (PSO) to optimize the operational performance of BESS. Jamroen et al. [25] proposed an adaptive droop-based method that takes into account the SoC system to manage the functioning of BESS in a low voltage (LV) system. The objective is to mitigate voltage rise caused by high solar penetration by enhancing voltage regulation and power-sharing efficiency using fuzzy logic.

The literature research revealed that the current instability of renewable energy poses a variety of issues. This study presents a solution to mitigate the impact of renewable energy on VD in ADN. The optimum BESS management is achieved by adopting a VDC approach that employs BESS to charge and discharge energy to the system. The adaptive droop control approach was chosen for BESS management because it allows the droop coefficient to be chosen as desired and appropriate, as well as taking into account the SoC level. In addition, the PSO is used to get the most appropriate droop coefficient value for battery control. The IEEE 33-bus test system was chosen as a test system because it is a distribution system with voltage levels lower than the standard criterion, making it acceptable for testing.

The following sections of this paper are organized as follows: Section 2 presents a mathematical analysis of BESS management. Section 3 provides an explanation of the voltage regulation technique developed with the PSO algorithm. Section 4 details the simulation analysis and results, while Section 5 concisely summarizes the conclusion.

2. BESS WITH ADAPTIVE VOLTAGE DROOP CONTROL

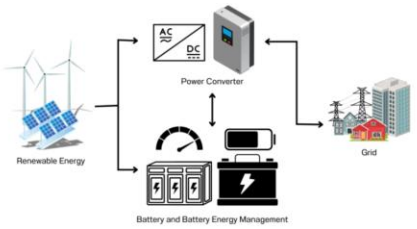

Fig. 1. BESS configuration

The BESS configuration is shown in Fig. 1, which includes the following main elements: a battery for storing energy, a battery energy management system for controlling BESS operation, and a power converter for energy conversion.

In this study, we focus on the battery and its energy management system. This study presents a method for controlling battery operations to resolve the VD issue. The battery can either provide or receive active power from the grid. When the BESS supplies active power to the grid, the voltage level rises, whereas when it absorbs active power from the grid, the voltage level drops. Thus, the BESS's operation can affect the voltage when the active power changes. Therefore, effective BESS operation relies heavily on battery energy management. According to a review, Fig. 2 shows that the VDC has three modes: (1) Mode 1 (Fixed Voltage): Keeps the voltage at a predetermined level and allows the battery power to adjust as needed, (2) Mode 2 (Fixed Power): Keeps the battery's power output constant, (3) Mode 3 (Droop Control): Uses a droop coefficient to determine how much power the battery delivers or consumes depending on the grid voltage.

This study uses the droop control method (Mode 3) to regulate battery operation because it can adjust the droop coefficient, allowing the voltage level to be freely regulated [24], [26]. Fig. 3 illustrates the operating concept as follows:

• 1: If the bus voltage of the battery exceeds the maximum voltage ($V_{\max}$), the battery will charge the maximum power into the system.
• 2: If the bus voltage value of the battery is less than the maximum voltage ($V_{\max}$) but larger than the maximum voltage thresholds ($V_{\text{th}}^{\max}$), the battery will charge power based on VD, which is governed by the droop coefficient.
• 3: If the battery's bus voltage value falls within the range of the minimum voltage thresholds ($V_{\text{th}}^{\min}$) and the maximum voltage thresholds ($V_{\text{th}}^{\max}$) or the deadband range, the battery will not charge or discharge at all.
• 4: If the bus voltage value of the battery is larger than the minimum voltage ($V_{\min}$) but less than the minimum voltage thresholds ($V_{\text{th}}^{\min}$), the battery will discharge the power based on VD, which is governed by the droop coefficient.
• 5: If the battery's bus voltage value is less than the minimum voltage ($V_{\min}$), it will discharge the maximum power back.

It can be represented mathematically as an equation given below:

$$P_{BES} = \begin{cases} -P_{BES}^{\max} & \text{if } V_i \geq V^{\max} \\ k_{BES,c(SoC)}\Delta V & \text{if } V_{\text{th}}^{\max} < V_i < V^{\max} \\ 0 & \text{if } V_{\text{th}}^{\min} \leq V_i \leq V_{\text{th}}^{\max} \\ k_{BES,d(SoC)}\Delta V & \text{if } V^{\min} < V_i < V_{\text{th}}^{\min} \\ P_{BES}^{\max} & \text{if } V_i \leq V^{\min} \end{cases} \quad (1)$$

$$\Delta V = V_i - V_0 \quad (2)$$

Since the battery may be saturated, it cannot be utilized further, causing the system to have a VD value that exceeds the required limit. As a result of the investigation, the SoC level was examined, as shown in the equation below.

$$k_{BES,d} = \begin{cases} 0 & \text{if } 0 < \text{SoC} \leq \text{SoC}_{\min} \\ \dfrac{K_{\max}K_{\min}e^{n_d(SoC-SoC_{\min})}}{K_{\max}+K_{\min}e^{n_d(SoC-SoC_{\min})}-1} & \text{if } \text{SoC}_{\min} < \text{SoC} \leq 1 \end{cases} \quad (3)$$

$$k_{BES,c} = \begin{cases} 0 & \text{if } \text{SoC}_{\max} \leq \text{SoC} < 1 \\ \dfrac{K_{\max}K_{\min}e^{n_c(SoC_{\max}-SoC)}}{K_{\max}+K_{\min}e^{n_c(SoC_{\max}-SoC)}-1} & \text{if } 0 < \text{SoC} < \text{SoC}_{\max} \end{cases} \quad (4)$$

$$SoC(t) = SoC(t-1) - \frac{1}{E}\int P_{BES}(t)dt \quad (5)$$

$$k_{droop} = \begin{cases} k_{BES,c}, \text{ charging} \\ k_{BES,d}, \text{ discharging} \end{cases} \quad (6)$$

$$n = \begin{cases} n_c, \text{ charging} \\ n_d, \text{ discharging} \end{cases} \quad (7)$$

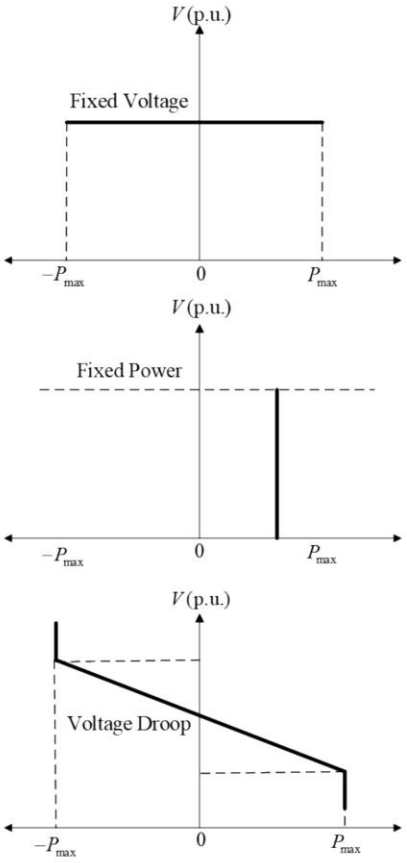

Fig. 2. VDC strategies

When evaluating k_{droop}, it is discovered that this value is related to the determination of $K_{\max}$, $K_{\min}$, SoC, and n As a result, while examining (1), (3), and (4), it can be represented in Fig. 4 and 5. From Fig. 4, it has been discovered that as the SoC of the battery increase, the $k_{BES,d}$ value gradually increases, the $k_{BES,c}$ value gradually decrease. This is because adaptive droop management is intended to protect the battery's

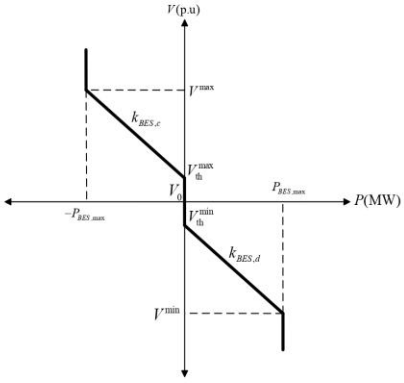

Fig. 3. Adaptive VDC strategy

functionality, which increases the SoC range, resulting in less charging and discharging. On the other hand, a low SoC level in the battery causes it to charge more and discharge less. The aforementioned relationship leads to the design of $K_{\max}$, $K_{\min}$ and n values, demonstrating that $K_{\max}$ and $K_{\min}$ will have a relationship with the desired power output, and n will be the factor determining the battery's power distribution, which is related to SoC, as shown in Fig. 5.

3. PSO BESED VOLTAGE DEVIATION IMPROVEMENT

PSO is a well-known metaheuristic method that mimics bird group's foraging activity. It accomplishes this by altering the locations of particles in search space, directing them toward the best solution discovered, similar to birds following the individual closest to a food source until the food is reached. Consequently, PSO is adept at determining optimal settings by iteratively updating particle positions.

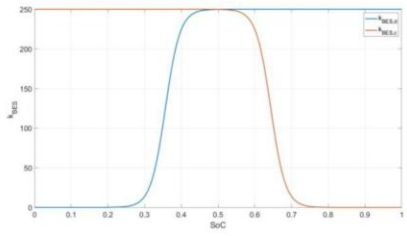

Fig. 4. The Relationship between SoC and k_{BES} with the SoC is within the range of $SoC_{\min}$ and $SoC_{\max}$

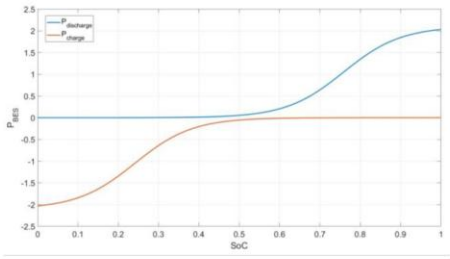

Fig. 5. The Relationship between SoC and n with the SoC is within the range of $SoC_{\min}$ and $SoC_{\max}$

Each parameter or particle updates its position iteratively until reaching the optimal value. The highest-performing value identified within the swarm is termed the global best, or $gBest$, while the best value found by an individual particle is known as the personal best, or $pBest_i$ [27]. This study uses PSO to change the adjustment exponent and calculate the droop efficient value, which is connected to battery operation, leading to the most efficient procedure based on the defined objective function.

This study aims to minimize the system's total voltage deviation (TVD) through the objective function. By reducing the TVD, the stability of the power system can be greatly enhanced. The objective function employed in this study is shown in the following equation.

$$\text{minimize } TVD = \sum_{i=1}^{N} (|V_i - V_0|) \tag{8}$$

and the constraints are defined as follows:

$$P_k^{gen} - P_k^{load} - \sum_{j=1}^{N} [V_k V_j (G_{kj} \cos\theta_{kj} + B_{kj} \sin\theta_{kj})] = 0 \tag{9}$$

$$Q_k^{gen} - Q_k^{load} - \sum_{j=1}^{N} [V_k V_j (G_{kj} \sin\theta_{kj} - B_{kj} \cos\theta_{kj})] = 0 \tag{10}$$

$$V_{\min} \le V_i \le V_{\max} \tag{11}$$

$$SoC_{\min} \le SoC \le SoC_{\max} \tag{12}$$

$$P_{BES,\min} \le P_{BES} \le P_{BES,\max} \tag{13}$$

$$k_{BES,d}^{\min} \le k_{BES,d} \le k_{BES,d}^{\max} \tag{14}$$

$$k_{BES,c}^{\min} \le k_{BES,c} \le k_{BES,c}^{\max} \tag{15}$$

The working equation of PSO is as follows:

$$v_i^{t+1} = wv_i^t + c_1 r_1 (pBest_i^t - x_i^t) + c_2 r_2 (gBest^t - x_i^t) \quad (16)$$

$$x_i^{t+1} = x_i^t + v_i^t \quad (17)$$

where x_i is the population of particles that represent the adjust exponent of $k_{BES,d}$ and $k_{BES,c}$, which are n_d and n_c, respectively. The proposed PSO-based VD improvement computational procedure is illustrated in Fig. 6.

4. RESULTS AND DISCUSSION

The test was conducted on the IEEE 33-bus system, which includes one generator bus and 32 load buses, where bus 1 is designated as the slack bus. The system's voltage restrictions range from 0.9 to 1.1 p.u. The system contains 3.715 MW of real power load and 2.3 MVar of reactive power load. The substation's nominal voltage is configured at 13.8 kV, with the transformer at bus 1 having a capacity of 3 MW. [28], [29]. In the simulation, the experiment is conducted as a single fixed-load test.

Table 1 also provides the study's parameters, which were evaluated and adjusted as needed, mostly through trial and error. The battery size was selected by using trial-and-error to adjust parameters, so they suit the operation of the IEEE 33-bus power system under both non-renewable and renewable energy conditions. From these trials, it was found that a 2 MWh size is appropriate for this system. The variable n specifies how quickly the battery can charge or discharge. A larger n allows faster charging or discharging when the BESS SoC is near its maximum or minimum, whereas a smaller n slows charging or discharging when the BESS SoC is near the nominal level. Therefore, we conducted trials to adjust these ranges, as illustrated in Fig 5.

The test is divided into three scenarios, as follows:

- case I: base case,
- case II: modified IEEE 33-bus with PV and wind power penetration, and
- case III: modified IEEE 33-bus with PV and wind power penetration and BESS with optimal VDC.

The system with renewable energy and BESS is shown on Fig. 7.

4.1 IEEE 33-bus base case

An initial test was conducted on an IEEE 33-bus distribution system. The voltage of each bus in the system ranges from 0.9038 p.u. to 1.0000 p.u., and the TVD is 1.8047 p.u., This significant deviation indicates that the bus voltages are not within the typical standard range of 0.95 p.u. to 1.05 p.u. The bus with the lowest value is Bus 18. Consequently, the lower-voltage bus should be prioritized to prevent power system instability, which could potentially lead to blackouts.

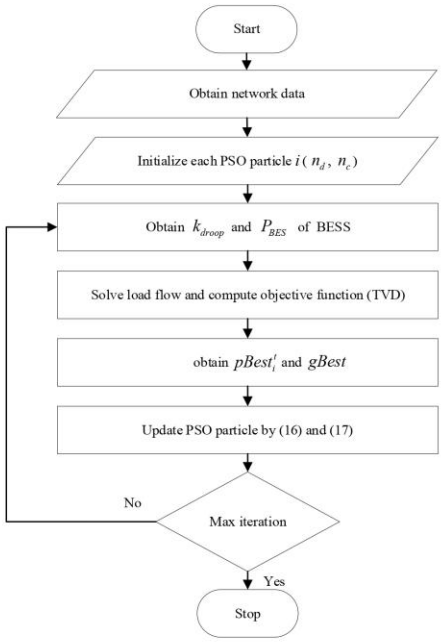

Fig. 6. The PSO based BESS optimal VDC computation procedure

Table 1. Specification of the BESS

Parameter	Specification
Range of the adjust exponent (n_d , n_c)	-100 to 100
The maximum power of battery ($P_{BES}^{\max}$)	2 MW
The maximum droop coefficient ($K_{\max}$)	250
The minimum droop coefficient ($K_{\min}$)	0.1
Nominal Voltage (V_0)	1.00 p.u.
Battery capacity (E)	2 MWh
The maximum voltage ($V_{\max}$)	1.10 p.u.
The minimum voltage ($V_{\min}$)	0.90 p.u.
Maximum state of charge ($SoC_{\max}$)	0.8 p.u.
Minimum state of charge ($SoC_{\min}$)	0.2 p.u.

4.2 *Modified IEEE 33-bus with PV and wind power penetration*

In this study, PV and wind power, as renewable energy sources, were integrated into an IEEE 33-bus distribution network. Two 1 MW wind turbine generators were installed at buses 18 and 24. Additionally, three 1 MW PV systems were deployed at buses 5, 21, and 31, while four 500 kW PV systems were positioned at buses 8, 12, 28, and 33 [30]. As a result of these renewable energy installations, the system's real power increased to 10.715 MW. It was observed that the system voltage ranged from 1.0000 p.u. to 1.0534 p.u. and that TVD was 0.6879 p.u. These findings indicate that high levels of renewable energy penetration impact the power system, causing over voltages and significant voltage fluctuations that negatively affect the electrical network. Therefore, appropriate energy management strategies should be implemented.

4.3 *Modified IEEE 33-bus with PV and wind power penetration and BESS with optimal VDC.*

In case III, the proposed method incorporates a battery into the system and employs PSO to optimize the system to obtain the best value that minimizes TVD. The PSO parameters are configured as follows w ranges from 0.1 to 1.1, both c_1 and c_2 are set to 1.49 and the maximum iterations is 100, which was selected through multiple trial runs. It was observed that the values generally start to converge around iterations 20-50, so this value was set accordingly. A 2 MWh battery has been installed on buses 18, 21, 24, and 32. The results show that the voltage levels on all buses in the system are within the prescribed range, with TVD being 0.0385 p.u. This adjustment was made using the variables presented in Table 2, specifically the values of the adjust exponent (n), droop coefficient (k_{droop}) and regulating power (P_{BES}) for each battery. The sign of P_{BES} for each value indicates whether the battery is charging or discharging. Specifically, a negative sign denotes that the BESS is charging, whereas a positive sign signifies that it is discharging.

Figure 8 illustrates the voltage profile for all three scenarios, showing that the proposed method maintains the voltage profile within the specified range through efficient battery charging and discharging. Table 3. depicts the 3 scenarios of TVD, indicating that the proposed method also

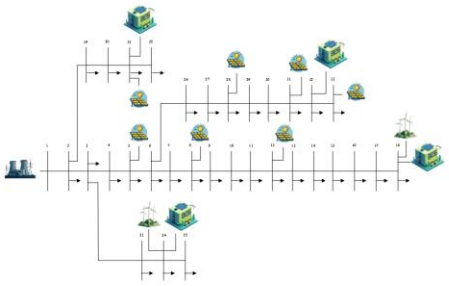

Fig. 7. The modified IEEE 33-bus with PV and wind power penetration and BESS

produces the best results by reducing VD compared to case 1 and 2. Furthermore, Fig. 9 shows the convergence plot of the proposed PSO-based BESS optimal VDC. it is clear that the value of the objective function progressively converges toward the optimal solution. Fig. 10 presents the results of 30 trials conducted using the proposed method that have the average value is 0.0409, standard deviation value is 0.0052, maximum value is 0.0524 and minimum value is 0.0385. The low standard deviation of the objective function values indicates that they are closely clustered, suggesting that the results obtained from PSO algorithm are reliable. The runtime of the proposed method was evaluated over 30 runs on a computer equipped with an AMD Ryzen 5 6600H CPU (3.30 GHz up to 4.50 GHz) and 16 GB of RAM. On average, the method took 774.45 seconds to complete, with a standard deviation of 178.33 seconds. The minimum runtime observed was 591.81 seconds, while the maximum reached 1490.75 seconds. Thus, although the PSO method typically requires about 774.45 seconds, it can occasionally take as long as 1490.75 seconds, likely due to unfavorable random initializations delaying convergence. These results are illustrated in Figure 11.

Table 2. Adjust exponent, Droop coefficient and BEES regulating power of BESS

Bus with Battery Installed	n	k_{droop}	P_{BES} (MW)
18	9.7258	12.3498	-0.6591
21	13.6507	67.4965	-0.6139
24	10.2878	16.0991	-0.0627
32	10.7010	19.5058	-0.5282

Table 3. Adjust exponent, Droop coefficient and BEES regulating power of BESS

Scenarios	TVD (p.u.)
IEEE 33-bus base case	1.8047
Modified IEEE 33-bus with PV and wind power penetration	0.6879
Modified IEEE 33-bus with PV and wind power penetration and BESS with optimal VDC.	0.0385

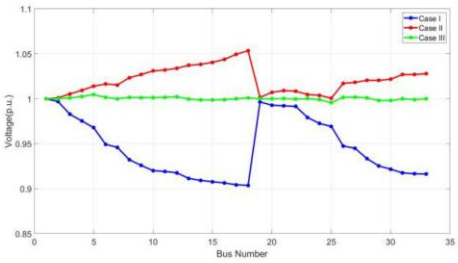

Fig. 8. Comparative Voltage Profile of modified IEEE 33-bus system

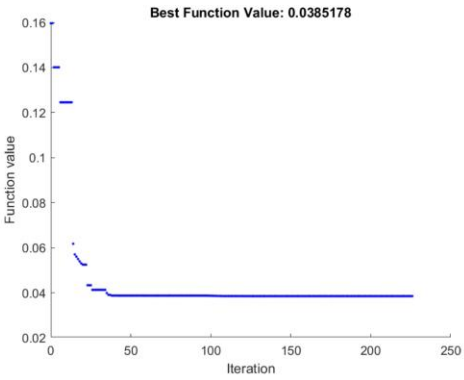

Fig. 9. the convergence plot of the proposed PSO-based BESS optimal VDC

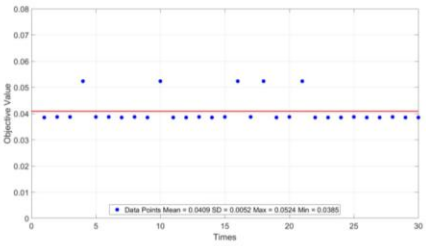

Fig. 10. The result of 30 trials of the proposed method

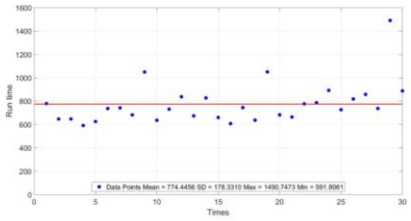

Fig. 11. The result of 30 trials of the computation time

5. Conclusion

This paper introduces a voltage regulation approach utilizing BESS management, tested on an IEEE 33-bus power distribution system. The primary goal is to determine the power value that will minimize TVD. The BESS management employed in this work is VDC, which is responsible for optimizing battery performance and responding to changes in electrical loads. In addition, the PSO approach is employed to determine the settings for BESS control. The results of this study indicate that the proposed method significantly reduces VD, resulting in a more stable power supply. Reducing voltage variation is critical for sustaining power quality and reliability across the power system.

ABBREVIATIONS

P_{BES}	The electrical power that a battery charges or discharges
$P_{BES}^{\max}$	The maximum power that the battery can supply.
k_{droop}	The droop coefficient
$k_{BES,c}$	The droop coefficient controls energy charge.

$k_{BES,d}$	The droop coefficient controls energy discharge.
ΔV	voltage deviation
V_i	Bus voltage
V_0	Nominal voltage
TVD	Total voltage deviation
$V_{\text{th}}^{\max}$	The maximum voltage thresholds
$V_{\min}$	The minimum voltage
$V_{\max}$	The maximum voltage
$K_{\max}$	The maximum droop coefficient
$K_{\min}$	The minimum droop coefficient
n	The adjust exponent
n_d	The adjust exponent for $k_{BES,d}$
n_c	The adjust exponent for $k_{BES,c}$
$SoC(t)$	state of charge at the current step
$SoC(t-1)$	state of charge at the previous step
E	Battery capacity
N	Number of buses
SoC	State of charge
$SoC_{\min}$	Minimum state of charge
$SoC_{\max}$	Maximum state of charge
$P_{BES,\min}$	The minimum power that the battery can supply
$P_{BES,\max}$	The maximum power that the battery can supply
$pBest_i$	The best value of each particle i
$gBest$	The best value of all particles
t	The iteration
v_i	The velocity for a particle i
c_1 and c_2	Constant numbers
r_1 and r_2	Random parameters
w	Inertial weight
x_i	The population of particles i
P_k^{gen}	Active power generated at bus k
P_k^{load}	Active power consumed by the load at bus k
Q_k^{gen}	Reactive power generated at bus k
Q_k^{load}	Reactive power consumed by the load at bus k
G_{kj}	Conductance between bus k and j
B_{kj}	Susceptance between bus k and j
θ_{kj}	Phase angle difference between bus k and j

ACKNOWLEDGEMENTS

We would like to express our profound gratitude to Suranaree University of Technology for their invaluable assistance through scholarships and resources during this research project. Their extensive knowledge and unwavering support were instrumental in bringing this study to a successful conclusion.

REFERENCES

[1] Adetokun, B.B.; Muriithi, C.M.; Ojo, J.O.; and Oghorada, O. 2023. Impact assessment of increasing renewable energy penetration on voltage instability tendencies of power system buses using a QV-based index. Scientific Reports 13(1): 9782.

[2] Adegoke, S.A. and Sun, Y. 2023. Power system optimization approach to mitigate voltage instability issues: A review. Cogent Engineering 10(1): 2153416.

[3] Pachanapan, P.; Kaewchum, T.; and Somkun, S. 2023. Voltage Level Control by Grid-tied Hybrid Photovoltaic and Battery Controllers in Weak Distribution Networks with Electric Vehicles. GMSARN International Journal 17: 291-301.

[4] Pachanapan, P.; Tadthip, A.; and Somkun, S. 2021. Implementation of Single-Phase Grid-Tied Inverter with Voltage Controller for Preventing Over-Voltage Problem in Distribution Networks with Solar PV Rootftops. 15: 59-67.

[5] Sode-Yome, A.; Mithulananthan, N.; and Lee, K.Y. 2007. A Comprehensive Comparison of FACTS Devices for

Enhancing Static Voltage Stability. Proceedings of the 2007 IEEE Power Engineering Society General Meeting. 24-28 June 2007. pp. 1-8.

[6] Sarimuthu, C.; Ramachandaramurthy, V.K.; Ramasamy, A.; and Mokhlis, H. 2016. A review on voltage control methods using on-load tap changer transformers for networks with renewable energy sources. Renewable and Sustainable Energy Reviews 62: 1154-1161.

[7] Abedini, M.; Davarpanah, M.; Sepehr, A.; and Ajaei, F.B. 2020. Shunt capacitor bank: Transient issues and analytical solutions. International Journal of Electrical Power & Energy Systems 120: 106025.

[8] Gurav, P. and Mittal, S.K. 2016. Control of Voltage Regulation Using STATCOM. International Journal of Advanced Research in Electrical, Electronics and Instrumentation Engineering 5(6): 5589-5596.

[9] Xu, Y. and Li, F. 2014. Adaptive PI Control of STATCOM for Voltage Regulation. IEEE Transactions on Power Delivery 29(3): 1002-1011.

[10] Ahmed, H.M.A.; Awad, A.S.A.; Ahmed, M.H.; and Salama, M.M.A. 2020. Mitigating voltage-sag and voltage-deviation problems in distribution networks using battery energy storage systems. Electric Power Systems Research 184: 106294.

[11] Shi, Y.; Xu, B.; Wang, D.; and Zhang, B. 2018. Using Battery Storage for Peak Shaving and Frequency Regulation: Joint Optimization for Superlinear Gains. pp. 1-1.

[12] Shang, L.; Dong, X.; Liu, C.; and Gong, Z. 2022. Fast Grid Frequency and Voltage Control of Battery Energy Storage System Based on the Amplitude-Phase-Locked-Loop. IEEE Transactions on Smart Grid 13(2): 941-953.

[13] Mohammed, A.Q.; Al-Anbarri, K.A.; and Hannun, R.M. 2021. USING PARTICLE SWARM OPTIMIZATION TO FIND OPTIMAL SIZING OF PV-BS AND DIESEL GENERATOR. Journal of Engineering and Sustainable Development 25(3): 51-59.

[14] Saini, P. and Gidwani, L. 2022. An investigation for battery energy storage system installation with renewable energy resources in distribution system by considering residential, commercial and industrial load models. Journal of Energy Storage 45: 103493.

[15] Tamrakar, U.; Nguyen, T.A.; and Byrne, R.H. 2021. Model Predictive Dispatch of Energy Storage for Voltage Regulation in Active Distribution Systems. Proceedings of the 2021 IEEE 30th International Symposium on Industrial Electronics (ISIE). 20-23 June 2021. pp. 1-6.

[16] Zhang, Q.; He, J.; and Zhang, D. 2017. Coordinated control of energy storage devices and photovoltaic inverters for voltage regulation based on multi-agent system. Proceedings of the 2017 IEEE Conference on Energy Internet and Energy System Integration (EI2). 26-28 Nov. 2017. pp. 1-6.

[17] Alam, M.J.E.; Muttaqi, K.M.; and Sutanto, D. 2013. Mitigation of Rooftop Solar PV Impacts and Evening Peak Support by Managing Available Capacity of Distributed Energy Storage Systems. IEEE Transactions on Power Systems 28(4): 3874-3884.

[18] Tandon, A.; Jain, P.; Gauta, T.; Yadav, Y.; Arya, S.; and Solanki, Y. 2024. Battery Energy Storage System Allocation in the IEEE 33 Bus Test System for enhanced system performance. E3S Web of Conferences 559.

[19] Alzahrani, A.; Alharthi, H.; and Khalid, M. 2023. Minimization of Power Losses through Optimal Battery Placement in a Distributed Network with High Penetration of Photovoltaics. Energies 13(1).

[20] Wang, Y.; Tan, K.T.; Peng, X.Y.; and So, P.L. 2016. Coordinated Control of Distributed Energy-Storage Systems for Voltage Regulation in Distribution Networks. IEEE Transactions on Power Delivery 31(3): 1132-1141.

[21] Rouzbehi, K.; Miranian, A.; Candela, J.I.; Luna, A.; and Rodriguez, P. 2015. A Generalized Voltage Droop Strategy for Control of Multiterminal DC Grids. IEEE Transactions on Industry Applications 51(1): 607-618.

[22] Zeraati, M.; Hamedani Golshan, M.E.; and Guerrero, J. 2016. Distributed Control of Battery Energy Storage Systems for Voltage Regulation in Distribution Networks With High PV Penetration. IEEE Transactions on Smart Grid PP: 1-1.

[23] Chen, X.; Wang, L.; Sun, H.; and Chen, Y. 2017. Fuzzy Logic Based Adaptive Droop Control in Multiterminal HVDC for Wind Power Integration. IEEE Transactions on Energy Conversion 32(3): 1200-1208.

[24] Jamroen, C. and Sirisukprasert, S. 2022. A voltage regulation strategy with state of charge management using battery energy storage optimized by a self-learning particle swarm optimization. Computers and Electrical Engineering 101: 108103.

[25] Jamroen, C.; Pannawan, A.; and Sirisukprasert, S. 2018. Battery Energy Storage System Control for Voltage Regulation in Microgrid with High Penetration of PV Generation. Proceedings of the 2018 53rd International Universities Power Engineering Conference (UPEC). 4-7 Sept. 2018. pp. 1-6.

[26] Tan, Z.; Li, X.; He, L.; Li, Y.; and Huang, J. 2020. Primary frequency control with BESS considering adaptive SoC recovery. International Journal of Electrical Power & Energy Systems 117: 105588.

[27] Freitas, D.; Lopes, L.G.; and Morgado-Dias, F. 2020. Particle Swarm Optimisation: A Historical Review Up to the Current Developments. Entropy 22(3).

[28] Isong, U.; Okpura, N.; and Oritsetimeyin Tim, P. 2023. The IEEE 33 Bus Distribution System Load Flow Analysis Using Newton Raphson Method. 10: 2458-9403.

[29] Baran, M.E. and Wu, F.F. 1989. Network reconfiguration in distribution systems for loss reduction and load balancing. IEEE Transactions on Power Delivery 4(2): 1401-1407.

[30] Jayasekara, N.; Masoum, M.A.S.; and Wolfs, P.J. 2016. Optimal Operation of Distributed Energy Storage Systems to Improve Distribution Network Load and Generation Hosting Capability. IEEE Transactions on Sustainable Energy 7(1): 250-261.